Tectonophysics 532–535 (2012) 61–81

Contents lists available at SciVerse ScienceDirect

Tectonophysics

journal homepage: www.elsevier.com/locate/tecto

Review Article

Systematic comparisons of earthquake source models determined using InSAR and seismic data

Jennifer Weston [a,*], Ana M.G. Ferreira [a,b], Gareth J. Funning [c]

[a] School of Environmental Sciences, University of East Anglia, Norwich, UK
[b] ICIST, Instituto Superior Técnico, Technical University of Lisbon, Lisbon, Portugal
[c] Department of Earth Sciences, University of California, Riverside, USA

ARTICLE INFO

Article history:
Received 31 May 2011
Received in revised form 30 January 2012
Accepted 2 February 2012
Available online 21 February 2012

Keywords:
InSAR
Seismology
Earthquake source parameters
Joint inversions
Spatial geodesy

ABSTRACT

Robust earthquake source parameters (e.g., location, seismic moment, fault geometry) are essential for reliable seismic hazard assessment and the investigation of large-scale tectonics. They are routinely estimated using a variety of data and techniques, such as seismic data and, more recently, Interferometric Synthetic Aperture Radar (InSAR). Comparisons between these two datasets are frequently made although not usually in a comprehensive way. This review compares source parameters from global and regional seismic catalogues with those from a recent database of InSAR parameters, which has been expanded with 18 additional source models for this study.

We show that moment magnitude (M_w) estimates agree well between the two datasets, with a trend for thrust events modelled using InSAR to have slightly larger M_w estimates. Earthquake locations determined using InSAR agree well with those reported in regional catalogues, with a median difference of 6.3 km between them, which is smaller than for global seismic catalogues. We also investigate the consistency of source parameters and source directivity by comparing ISC hypocentres with GCMT and ICMT centroid locations for earthquakes with $M_w \geq 6.5$. In some cases the source directivity is qualitatively comparable with previous studies, especially when comparing ISC and ICMT locations. The average difference between InSAR-determined depths and those in the EHB catalogue is reduced if a layered half-space is used in the inversion of InSAR data. Overall, faulting geometry (strike, dip and rake angles) remain in good agreement with values from the GCMT catalogue, and any large discrepancies can be attributed to tradeoffs between parameters. With continued investment in satellites for radar interferometry, InSAR is a valuable technique for the estimation of earthquake source parameters. The observed trends and discrepancies between InSAR and seismically determined source parameters are the result of issues with the data, different inversion techniques and the assumed Earth structure model.

Contents

* Corresponding author.
E-mail address: J.weston@uea.ac.uk (J. Weston).

0040-1951/$ – see front matter © 2012 Elsevier B.V. All rights reserved.
doi:10.1016/j.tecto.2012.02.001

1. Introduction

Seismic data are routinely used to determine source models for earthquakes and, increasingly, Interferometric Synthetic Aperture Radar (InSAR) data are also being used. Each dataset has its own strengths and weaknesses, which complement each other when jointly inverted, but only a few studies have compared results from the two datasets (e.g., Funning, 2005; Lohman et al., 2002; Mellors et al., 2004; Weston et al., 2011; Wright et al., 1999). Although there is generally good agreement between the source parameters for the majority of earthquakes previously studied, differences in location, seismic moment and fault geometry have highlighted issues including the Earth model used and the quality of the data. Gaining an understanding of these issues enables the development of inversion techniques of both InSAR and seismic data for the calculation of more robust source models.

Robust earthquake source models are important for studying kinematic and dynamic processes at the fault scale all the way up to the tectonic scale. At the fault scale, errors in source models affect the interpretation of stress regimes, seismogenic depth and fault structure in the area, all of which are important for seismic hazard assessment (Mellors et al., 2004). Currently there is not a homogeneous catalogue of InSAR-determined earthquake source parameters, whereby the source models have been determined using consistent modelling techniques and Earth models. There are, however, many seismic catalogues, and the source mechanisms from them can provide vital information regarding the tectonic stresses and regimes in a region (e.g., the Regional Centroid Moment Tensor Catalogue (RCMT), Pondrelli et al., 2002).

Comparisons between InSAR and seismically determined source models provide insights into the tradeoffs and uncertainties of the source parameters determined from the inversion of both datasets. This, and issues related to the data itself and the processing and inversion techniques used will be discussed in this review, following a short summary of the two techniques.

2. Investigating earthquakes using InSAR data

InSAR is a space geodetic technique that allows the surface displacements caused by an earthquake to be mapped remotely. Elastic dislocation models can then be used to match the pattern of measured displacements and thus obtain source parameters of the event. The first earthquake successfully detected and modelled using InSAR data was the Landers event (28th June 1992, M_w 7.3, Massonnet et al., 1993) and since then the number of seismic events investigated using geodetic data has steadily increased. InSAR is another valuable tool for providing constraints on earthquake source parameters, having the advantage of strong spatial resolution in comparison with seismic data; e.g., it is generally possible to visually identify the location of earthquake faults in the interferogram without the need for any modelling.

2.1. Principles and progress of the technique

There are many studies which have reviewed the principles of InSAR (e.g., Burgmann et al., 2000; Feigl, 2002; Massonnet and Feigl, 1998) and these should be referred to for a more detailed discussion, but an overview of the technique will be outlined here.

Synthetic Aperture Radar (SAR) involves a moving side-looking radar emitting pulses of microwave radiation towards the ground and measuring the amplitude and phase of the radiation that is scattered back to the radar. By combining responses from multiple observation points as the radar platform moves, a high resolution SAR image is obtained (a comprehensive overview of SAR imaging can be found in e.g., Curlander and McDonough, 1991). InSAR is based on the difference in phase between two SAR images; if these two SAR images are acquired before and after an earthquake, part of the phase difference corresponds to a one-dimensional measure of the surface deformation in the satellite line-of-sight direction. However, atmospheric delay, topography and the difference in satellite position at the two image acquisition times can also cause phase changes.

In order to isolate the phase change due to the earthquake surface displacement several methods have been developed to remove the other contributing factors, which are usually carried out during the data processing stage. Interferometric fringes due to topography are removed using a Digital Elevation Model (DEM) and the phase shift due to a change in satellite position can be corrected by using knowledge of the satellite orbits. However, the phase delay due to the atmosphere is more difficult to remove and, unlike topography and orbital changes, is not routinely removed at present. In recent years there has been an increased focus on developing techniques for removing this remaining, and potentially major, source of error in radar interferometry. Approaches to calculate the delay include using meteorological or atmospheric models and observed data to calculate the potential contribution of the atmosphere, particularly water vapour (e.g., Doin et al., 2009; Pussegur et al., 2007; Wadge et al., 2010). Few studies have tried to integrate a method of removal into a processing routine for InSAR data, Li et al. (2005) successfully integrated water vapour correction models into the ROI_PAC (Rosen et al., 2004) software, a free and popular SAR data processing package.

Even in situations when such error sources are mitigated, noise from temporal decorrelation (changes to the radar scattering characteristics of the ground) can still remain in the interferogram. Changes in land use, land cover (e.g., snow) or vegetation can be responsible for decorrelation, and the probability of change, and thus decorrelation, increases with time. Decorrelation can be mitigated by using a long radar wavelength (e.g., the ALOS satellite, $\lambda = 235$ mm), which is able to penetrate the canopies of trees and scatter off their more stable trunks, and is less sensitive in general to changes in small scatterers on the ground.

There are three satellite missions currently in operation which provide radar images that can be used to produce interferograms (Table 1). The ERS-1 satellite from the European Space Agency

Table 1
Summary of past and present satellites that provide SAR data for the measurement of earthquakes. Note that COSMO-SkyMed is not one satellite but a constellation of four satellites.

Satellite	Operation period	Wavelength (mm)	Band
European Remote Sensing Satellite 1 (ERS-1)	1991–2000	56.7	C
European Remote Sensing Satellite 2 (ERS-2)	1995–2011	56.7	C
ENVISAT	2002–	56.3	C
Japanese Earth Resource Satellite (JERS-1)	1992–1998	235.0	L
Advanced Land Observation Satellite (ALOS)	2003–2011	235.0	L
COSMO-SkyMed	2007–	31.0	X
TerraSAR-X	2007–	31.0	X

(ESA) was the first to provide data that were used to measure the surface displacement caused by an earthquake, but it has been decommissioned since 2000. The ESA launched two further satellites, ERS-2, which has also been decommissioned and ENVISAT, which is nearing the decommission stage and consequently the agency plans to launch two new satellites as part of the project Sentinel. The first satellite to be launched in 2013, Sentinel-1A, is one of two C-band satellites which aim to continue collecting the type of data that the ENVISAT satellite currently provides (ESA, 2007, 2011). Theoretically the data should be of better quality than that collected by its predecessors due to the shorter time period between measurements (12 days; 6 days once Sentinel-1B is launched) and shorter baselines due to tighter orbital control.

InSAR can cover remote areas where seismic networks are limited but up to now there have been only a limited number of satellites, which have to be in the 'right place at the right time' to acquire images that can be used. Since 1992, the volume and accessibility of InSAR data has steadily increased and consequently the number of earthquakes studied using this type of data has increased also. There are now over 60 earthquakes that have been studied using InSAR data, a number sufficient to study the statistics of such events, as we demonstrate in Section 4.

There are various packages available for the processing of SAR data to produce interferograms. Fig. 1a shows an interferogram produced from ERS-1 SAR images, from descending track 442, processed using one of these packages — ROI_PAC (Rosen et al., 2004). It shows a very clear signal for the Eureka Valley earthquake (M_w 6.1, 17th May 1993) from which displacements with millimetre precision can be determined. Detailed overviews of the processing stages used in the programme are available in several other studies (e.g., Rosen et al., 2000, 2004) but the process will be briefly summarised here. The two SAR images are preprocessed to produce Single-Look Complex images (SLC), which are high resolution images that contain both the phase and amplitude information. Then, using orbital information, the SLC images are resampled into the same geometry and the image acquired before the earthquake is multiplied by the complex conjugate of the 'after' image to form the interferogram. The signal from topography is then removed by calculating a synthetic interferogram using orbital information and the DEM (e.g., 1 arc second Shuttle Radar Topography Mission (SRTM) data). The interferogram is then filtered to enhance the strongest signals and the phase part of the signal is unwrapped from its modulo 2π values into a continuous function to give the total phase shift in the path between the ground and the satellite. This unwrapped interferogram is then used to refine the viewing geometry and thus refine the orbital and topographic corrections and, finally, the interferogram is geocoded to produce the image seen in Fig. 1a.

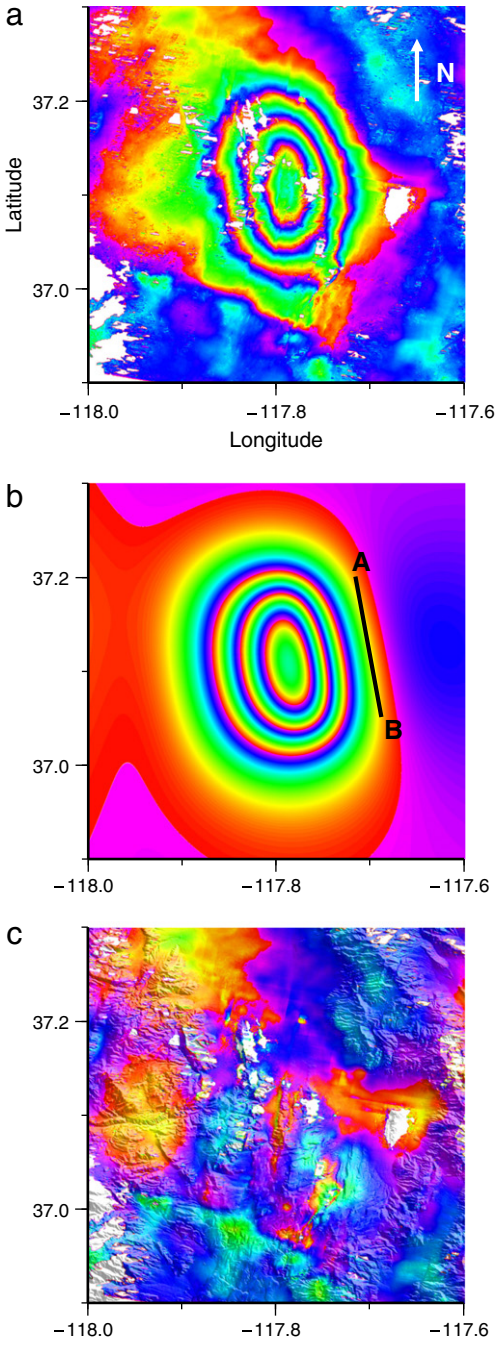

Fig. 1. a) Unwrapped interferogram showing a signal from the Eureka Valley earthquake (M_w 6.1, 17th May 1993). This was produced using two SAR images from 01/06/92 and 08/11/93. b) Synthetic interferogram, forward modelled using the source parameters listed in Table 2, where one colour cycle corresponds to 0.028 m of displacement. The black line shows the top of the fault projected up-dip to the surface, where A and B denote the ends of the fault. c) Residual interferogram, showing the difference between a) and b).

2.2. Modelling surface deformation using InSAR

Once an interferogram covering the earthquake is produced, the next step is to down-sample the highly spatially correlated data because with a small subset of the data it is still possible to model the key features of the data. Downsampling methods such as quadtree decomposition (e.g., Jonsson et al., 2002; Simons et al., 2002), focused near-field sampling (e.g., Funning et al., 2005), and resolution-based sampling (e.g., Lohman and Simons, 2005b) have all been successfully

used to reduce the number of data points to model from millions to hundreds-of-thousands.

Once down-sampled, the data can be inverted to determine source parameters that explain the observed surface deformation. This can be achieved using elastic dislocation theory, for example the mathematical expressions developed by Okada (1985), which relate slip on a rectangular dislocation, representing a fault in an elastic half-space, to surface displacements. The inversion for fault parameters (e.g., strike, dip, location and depth) from surface displacement data is a non-linear inverse problem, which can be solved by repeatedly computing a forward model of the surface displacements, and adjusting the fault parameters until the misfit between the modelled and the observed displacements is minimised. This can be achieved with a non-linear optimisation algorithm used to vary the source parameters systematically to find the solution with the best fit to the data. In one example such an algorithm is run multiple times (usually 100 to 1000) restarting with different initial parameters each time to produce a range of solutions with a range of minimum misfits, where the best solution corresponds to the overall lowest minimum misfit, or global minimum misfit (e.g., Funning, 2005; Wright et al., 1999).

We have followed this approach, using a curvature-based quadtree algorithm to downsample the data and determine a set of source of parameters for the Eureka Valley earthquake (Table 2). When forward modelled this solution produces the observed pattern of displacement seen in the synthetic interferogram in Fig. 1b. These modelled displacements are then subtracted from those that have been observed to produce a residual interferogram, which reveals how well the solution explains the observed deformation. The residual interferogram in Fig. 1c shows randomly distributed noise, which indicates that the model source parameters explain the InSAR data well. If this were not the case then information from the residual could be used to further refine the source model parameters.

It is common for InSAR data to be jointly inverted with other datasets such as seismic data (e.g., Pritchard et al., 2006) and GPS data (e.g., Fialko, 2004) or both (e.g., Delouis et al., 2002), which provides additional constraints and helps reduce the tradeoffs between certain parameters, an important issue discussed in Section 4, below.

3. Seismological modelling of earthquakes

With extensive global seismic networks deployed worldwide and vast data analysis and inversion techniques available, seismology is a well established and reliable technique for determining earthquake source parameters. Indeed, until the advent of satellite geodetic techniques it was the only means of doing so without undertaking fieldwork in the epicentral region of an earthquake. Consequently, there are many seismic catalogues (see Section 3.1) providing a rich source of information for many research areas, including seismic hazard assessment and tectonic studies.

The large volume of information that a seismogram represents means that there are a variety of ways in which it can be exploited for the determination of earthquake source parameters. Firstly the type of seismic data used can be from local or global seismic networks, or a combination of the two. The portion and frequency content of the seismogram used for the inversion can also vary. It can include, for example, P and S-wave traveltimes (e.g., McCaffrey et al., 1991), or long-period body and surface waveforms (e.g., the Global Centroid Moment Tensor (GCMT) catalogue, Dziewonski et al., 1981).

For the fast inversion of seismic data, a point source can be assumed such as in the GCMT catalogue, or, if more information on the source is desired, a finite fault model can be determined (e.g., Wald and Heaton, 1994). There are strengths and weaknesses to each method, a discussion of which is outside the scope of this review, but the inversion methods employed in the seismic catalogues used here will now be outlined.

Table 2
Summary of source parameters for the Eureka Valley earthquake from three studies; Massonnet and Feigl (1995); Peltzer and Rosen (1995), this study, and from the Global Centroid Moment Tensor catalogue. The latitude, longitude and depth refer to the centroid location.

Parameter	Massonet and Feigl	Peltzer and Rosen	This study	GCMT
M_w	6.10	6.11	6.06	6.10
Mo ($\times 10^{18}$ Nm)	1.70		1.55	1.83
Lat (°)	37.11		37.11	36.68
Lon (°)	242.21		242.18	241.90
Depth (km)	9.2	13.0	8.1	15.0
Strike (°)	173.0	7.0	172.0	210.0
Dip (°)	54.0	50.0	37.6	30.0
Rake (°)			−95.2	−93.0

3.1. Inversion methods and source catalogues

The GCMT catalogue is one of the most frequently used seismic catalogues and has calculated focal mechanisms for moderate to large events ($M \geq 5.0$) since 1976. Long-period body and surface waves are used in inversions for the six moment tensor components. Synthetic seismograms for each moment tensor component at each seismometer location, otherwise known as excitation kernels, are calculated using normal mode summation (e.g., Gilbert and Dziewonski, 1975) in a 3D earth model (SH8/U4L8, Dziewonski and Woodward, 1992). Originally, a 1D earth model was used instead (PREM, Dziewonski and Anderson, 1981). The observed seismograms can be expressed as a multiplication between the matrix of excitation kernels and the vector of six moment tensor components. To solve for the moment tensor this linear relationship is solved in a least-squares procedure. Once there is an initial estimate of the moment tensor, then excitation kernels are recalculated for all ten source parameters (centroid location, origin time and moment tensor) and an iterative least-squares inversion is carried out until an optimal agreement is reached between the observed and synthetic data (Dziewonski and Woodhouse, 1983; Dziewonski et al., 1981).

The International Seismological Centre (ISC) has two global catalogues; the ISC and EHB (Engdahl–van der Hilst–Buland) bulletins. The agency uses data from the monthly listing of events produced by the National Earthquake Information Centre (NEIC) and data submitted from various agencies around the world. These data are associated to an event and a least-squares procedure is used to determine four source parameters: hypocentral depth, location, and origin time. These parameters are reported in the ISC catalogue along with magnitude values m_b and M_s (Adams et al., 1982). To reduce the observed bias in ISC focal depths the methodology above was modified and a more recent earth model, the ak135 model (Kennett et al., 1995) was used instead of the Jeffreys and Bullen travel time tables (Jeffreys and Bullen, 1940). Station patch corrections and later phase arrivals were also incorporated into the procedure (Engdahl et al., 1998) and the resulting parameters are published in the EHB bulletin.

In addition to these global catalogues, there are numerous catalogues based on data from local or regional seismic networks, which focus on events in regions such as central Europe or individual countries, such as Japan. The following regional catalogues are used in this study:

- Regional Centroid Moment Tensor Catalogue (RCMT) — This reports source mechanisms for $4.5 < M < 5.5$ events in the Mediterranean region from 1997, with the most recently published catalogue including events up to 2008 (Pondrelli et al., 2011, 2010). The method used is the same as in the GCMT catalogue, except that in order to account for smaller magnitude events, the data are filtered at a low-pass filtered at 35 s to include shorter period fundamental mode surface waves. Synthetic seismograms for these waves are calculated using global laterally varying phase velocity models and propagating a source pulse through them (Pondrelli et al., 2002),

instead of a classical normal mode summation approach in a 1D Earth model.

- Euro-Med Bulletin — This has been developed, and is run by, the Euro-Mediterranean Seismological Centre (EMSC). The current database covers events in the Euro-Mediterranean region in the period 1998–2008. Data are collected from over 60 networks in 53 countries and the gathered phase and location information are processed in a three-step procedure to produce the bulletin. For a local event the associated phases are collected and a location is determined iteratively by computing travel times using a local velocity model until the least-square travel time residual is minimised. The location is then tested against the initial reported location, the variation in the travel time residual and the RMS, and the defining phases (Godey et al., 2006).
- National Research Institute for Earth Science and Disaster Prevention (NIED) Catalogue — There are several regional networks in Japan run by the Japan Meteorological Agency (JMA) and the NIED. The data are archived by JMA and NIED and made available for public use (Okada et al., 2004). For earthquakes since 1997 the data recorded on the regional broadband seismic network (F-net) have been used by the NIED to calculate focal mechanisms based on the polarities of the first P wave arrivals (Kubo et al., 2002).
- India Meteorological Department (IMD) Catalogue — Similar to Japan, regional data from their National Seismological Network (NSN) are used for the calculation of location and magnitude; the agency also submits the solutions to the ISC (IMD, 2011).
- Earthquake Mechanisms of the Mediterranean Area (EMMA) — This is a database of focal mechanisms for earthquakes that have occurred in the Mediterranean area between 1905 and 2003. The mechanisms and the related source parameters reported in the literature are collected as well as the data that were used to calculate them. The focal mechanisms are recomputed using these data and compared with the mechanism published in the study. Errors, such as rotations in strike or rake values as a result of the formulation used, are corrected for. Multiple solutions for one event are reported, but one is suggested as the best solution using a list of four criteria, the foremost dependent on whether errors were reported with the original solution; for further details see Vannuccii and Gasperini (2003).
- Advanced National Seismic System (ANSS) Composite Catalogue — This is a world-wide catalogue run by the Northern California Earthquake Data Center including events since 1898 to the present day. It merges solutions from 15 contributing regional networks across North America, and the NEIC. Each regional network is assigned a geographic region and solutions from this network for events that occur in the region are always reported in the catalogue. If multiple solutions from various networks are reported for an event, the solution from the network whose geographic region covers the location of the event is considered the best solution. For events with more than one solution that occur outside the area covered by the regional networks the solution with the largest magnitude is kept (ANSS, 2010).
- Southern California Seismic Network (SCSN) catalogue — Similar to ANSS, the Southern California Seismic Network (SCSN) collects data from regional seismic networks across North America, including its own network of over 160 stations. The origin time, date, location and magnitude along with uncertainties are determined using an automatic phase picking procedure and reviewed by a seismologist. There are currently over 470,000 events since 1932 to the present day included in the catalogue (Hutton et al., 2010).

4. Earthquake source parameter comparisons

Comparisons conducted in this review are made using the database in Weston et al. (2011) that has since been expanded with the events listed in Table 3 to include a total of 67 earthquakes from 1992 to 2010. The database (which will now be referred to as the InSAR Centroid Moment Tensor, or ICMT Catalogue) is a compilation of earthquake source parameters reported in studies which invert InSAR data or a combination of InSAR and other types of data such as GPS and seismic. Uniform and distributed slip models are included in the database and if the two types of model are published in a study and lead to equally good fit to the data, they are both included, unless the authors stated which is the preferred model. Often not all the required source parameters are given in the literature and where possible they have been calculated given the information in the study or from the authors when requested; for further details see Weston et al. (2011). One important parameter to note for Section 4.2, where we compare event locations with those determined seismically, is that the location given in our ICMT database refers to the centroid location, which is an average location if the earthquake is modelled as a point source with respect to seismic moment release. For uniform slip models this is taken to be the centre of the fault plane, but for variable slip models it is the spatial centroid obtained from the slip distribution; again, see our previous study for more details. The majority of the source parameter comparisons are made with solutions from the GCMT catalogue, except centroid depth, where comparisons are made with the EHB bulletin, and centroid location, where comparisons with regional catalogue locations are also included. It must be noted that locations given in the EHB and regional catalogues typically refer to the hypocentre (rupture initiation point), which is generally different from the centroid location and, although the two are not directly comparable this comparison can be informative; this issue is discussed further in Section 4.2.

4.1. Moment and moment-magnitude

Previous comparisons of InSAR and seismically determined seismic moment values have suggested that the InSAR derived seismic moment tends to be the larger of the two (Funning et al., 2007; Lohman and Simons, 2005a; Wright et al., 1999). Feigl (2002) reported differences of up to 60% between geodetically estimated and seismically estimated moments, but solutions from other types of geodetic data such as levelling and GPS were also included. The inclusion of interseismic, triggered aseismic and post-seismic deformation in coseismic interferograms due to the longer measurement periods of geodetic data, which can span years in some cases, were suggested as reasons for the trend and as such the moment estimates should increase with the measurement period.

However, our recent study of 58 earthquakes (Weston et al., 2011) has found the two datasets to agree well regarding the seismic moment, and a slight tendency for the moments calculated using InSAR data to be smaller than those reported in the GCMT catalogue. The addition of 18 new studies of nine individual events (Table 2) to the database in Weston et al. (2011) leaves the trend unchanged (Fig. 2). The median difference in moment magnitude (M_w) is still −0.009 magnitude units ($\sigma = 0.10$) and the cases where the InSAR moment magnitude is substantially larger are either due to contamination in the interferogram by deformation sources other than coseismic slip or poor InSAR data quality in general (Weston et al., 2011). Considering the difference in moment magnitude with respect to geographical location (Fig. 2a) there are no obvious regional biases towards InSAR-derived source models having higher or lower moments than the GCMT estimates, except for offshore of South America, where the ICMT moments appear systematically larger, an issue discussed in more detail later.

If the mechanism of the event is considered (Fig. 2b–d), then strike-slip and thrust events show the largest outlier discrepancies. Interestingly the large outliers in the strike-slip category are due to poor quality InSAR data regardless of whether the InSAR moment estimate is an over or underestimate with respect to seismic data. For

Table 3
Eighteen new earthquake source models that have been added to the existing database of Weston et al. (2011). Lat., Lon., and Depth refer to the centroid location. The faulting mechanism is defined in 'Type' column where ss, n and th refer to strike-slip, normal and thrust, respectively. The type of data used in each study is indicated in 'Data' I (InSAR data only), GI (GPS and InSAR data), and OI (InSAR data combined with two or more other types of data). Figures in bold have been fixed during the inversion. Several studies included more than one acceptable earthquake source model, and in some cases uniform and distributed slip models were obtained for the same event. Events with the suffix (ds) refer to distributed slip models.

Date	Location	Mo	Lat	Lon	Depth	Strike	Dip	Rake	Type	Data	Reference
		($\times 10^{18}$ Nm)	(°)	(°)	(km)	(°)	(°)	(°)			
22/12/99	Ain Temouchent, Algeria	0.47				57.0	32.0	90.0	th	I	(Belabbes et al., 2009a)
27/11/05	Qeshm Island, Iran	1.25 ± 0.01	26.88 ± 0.01	55.89 ± 0.004	5.80 ± 2.00	73.0 ± 3.10	36.0 ± 2.0	66.0 ± 5.0	th	I	(Nissen et al., 2010)
28/06/06	Qeshm Island, Iran	1.35 ± 0.32	26.91 ± 0.02	55.89 ± 0.004	8.50 ± 1.20	25.0 ± 11.0	46.0 ± 14.0	65.0 ± 17.0	th	I	(Nissen et al., 2010)
15/08/07	Pisco, Peru (ds)	2500.00							th	I	(Biggs et al., 2009)
15/08/07	Pisco, Peru (ds)	1230.00	−13.89	−76.77	19.07		8.0 to 27.0	64.8	th	I	(Motagh et al., 2008)
14/11/07	Tocopilla, Chile (ds)	501.00	−22.48	289.75	39.80	3.7	**20.0**	110.6	th	I	(Motagh et al., 2010)
09/01/08	Nima, Tibet	2.57	32.44	85.33	7.65	217.3 ± 1.4	60.0 ± 1.9	86.4	n	I	(Sun et al., 2008)
09/01/08	Nima, Tibet (ds)	5.40							n	I	(Sun et al., 2008)
12/05/08	Wenchuan, China (ds)	891.25	31.67	104.04	10.29	226.4	53.2	129.7	th	GI	(Feng et al., 2010)
12/05/08	Wenchuan, China (ds)	1536.24	31.77	104.23	7.47	228.2	48.7	156.0	th	OI	(Hao et al., 2009)
29/05/08	Iceland (doublet event)	1.46					**90.0**		ss	GI	(Decriem et al., 2010)
10/09/08	Qeshm Island, Iran	1.86 ± 0.18	26.88 ± 0.01	55.89 ± 0.01	5.80 ± 1.70	45.0	48.3 ± 7.6	53.8 ± 10.1	th	I	(Nissen et al., 2010)
06/04/09	L'Aquila, Italy	2.90	42.32	13.43	7.06	133.0 ± 2.0	47.0 ± 1.0	−103.0 ± 2.0	n	GI	(Atzori et al., 2009)
06/04/09	L'Aquila, Italy (ds)	2.70	42.32	13.43	6.20	**133.0**	**47.0**	**−103.5**	n	GI	(Atzori et al., 2009)
06/04/09	L'Aquila, Italy	2.80 ± 0.08	42.33 ± 0.001	13.45 ± 0.001	7.30 ± 0.10	144.0 ± 1.0	54.0 ± 1.0	−105.0 ± 3.0	n	I	(Walters et al., 2009)
06/04/09	L'Aquila, Italy (ds)	2.91	42.33	13.45	7.00	**144.0**	**54.0**	**−105.0**	n	I	(Walters et al., 2009)
19/12/09	Karonga, Malawi	1.40	−9.89	33.90	3.20	155.0	41.0	−88.0	n	I	(Biggs et al., 2010)
27/02/10	Maule, Chile (ds)	18,000.00	−35.87	287.08	29.75	**15.0**	**18.0**	**110.0**	th	OI	(Delouis et al., 2010)

example for the Al Hoceima event in 1994 (M_w 6.0) the InSAR estimate, based on a uniform slip model, is ~0.2 moment magnitude units larger than the GCMT estimate (M_w 6.0). This is due to tradeoffs between several parameters in the inversion, including length and seismic moment, as a result of an incomplete pattern of surface deformation in the interferogram because most of the displacement occurred offshore (Biggs et al., 2006). However, for thrust events, poor quality InSAR data can lead to substantially smaller InSAR derived moments. Significant decorrelation in interferograms due to dense vegetation and mountainous topography lead to InSAR moment magnitudes −0.31 and −0.1 smaller than those in the GCMT catalogue, for the Chamoli (M_w 6.2, 28th March 1999) and Bhuj (M_w 7.6, 26th January 2001) earthquakes, respectively (Satyabala and Bilham, 2006; Schmidt and Burgmann, 2006). In contrast, the ICMT moment magnitude is significantly larger than the GCMT estimate for two thrust events, Qeshm Island (M_w 5.8, 28th June 2006) and Pisco (M_w 8.0, 15th August 2007), which is likely due to the inclusion of additional, non-coseismic deformation in their associated interferograms.

Overall there is a slight trend for an overestimation of the moment magnitude for thrust events studied using InSAR (Fig. 2c). It has been suggested that the moment magnitude estimate from InSAR increases with the measurement period (e.g. Feigl, 2002). However, considering the length of the time period between the event and the measurement of the second SAR image for thrust events (now referred to as the post-seismic period) there is no clear trend (Fig. 3a). For 24 earthquake source models the ICMT moment is larger than that reported for the GCMT but the difference in moment shows widespread varation. The two overestimates previously highlighted (Qeshm Island and Pisco) have significantly different post-seismic periods; 659 days passed between the Qeshm Island earthquake and the acquisition of a second SAR image, whereas there was only a 65 day period between the Pisco earthquake and the 'after' SAR image.

We also investigate the influence of aftershocks. Fig. 3b shows the total seismic moment contribution from aftershocks reported in the GCMT catalogue that occurred in the post-seismic period covered by the interferogram, plotted as a fraction of the coseismic moment. As with the post-seismic period there is no evident trend and the largest contribution from aftershocks (~86%) in fact corresponds to a normal faulting event for which the ICMT and GCMT moment are in relatively good agreement (Colfiorito, M_w 5.6, 27th September 1997). There are two thrust events for which the ICMT moment is a significant overestimate with respect to that reported in the GCMT catalogue and there appears to be a significant contribution from aftershocks;~80% (Niigata, M_w 6.5, 24th October 2004) and ~54% (Qeshm Island, M_w 5.8, 28th June 2006). However, for the majority of thrust earthquakes where the ICMT moment is a significant overestimate with respect to the GCMT value, the relative contribution from aftershocks is small.

For several of the large subduction zone events in this study aftershocks account for much less than half of the estimated moment release during the observed post-seismic period. Afterslip on the subduction interface may at least partly be responsible for the additional moment release as reported contributions from this phenomenon vary from 60% (e.g., Antofagasta, M_w 8.1 30th July 1995; Chlieh et al., 2004) to 90% (e.g., Pisco M_w 8.0, 15th August 2007; Perfettini et al., 2010) of the overall moment release. Viscoelastic relaxation has also been suggested as potential mechanism for post-seismic deformation in the South American subduction zone. A total of 17 cm of horizontal trenchward motion was observed in the three and a half years following the Arequipa earthquake (M_w 8.5, 23rd June 2001), thought to be due to tensional stresses driving viscoelastic relaxation in the whole crust and the upper mantle (Hergert and Heidbach, 2006). Moving away from the subduction zone setting similarly high levels of afterslip (nearly 95% of the total observed post-seismic) were observed in the 1500 days following the Kashmir earthquake (M_w 7.6, 8th October 2005). The total post-seismic moment release was 56% ± 19% of the coseismic moment release, which

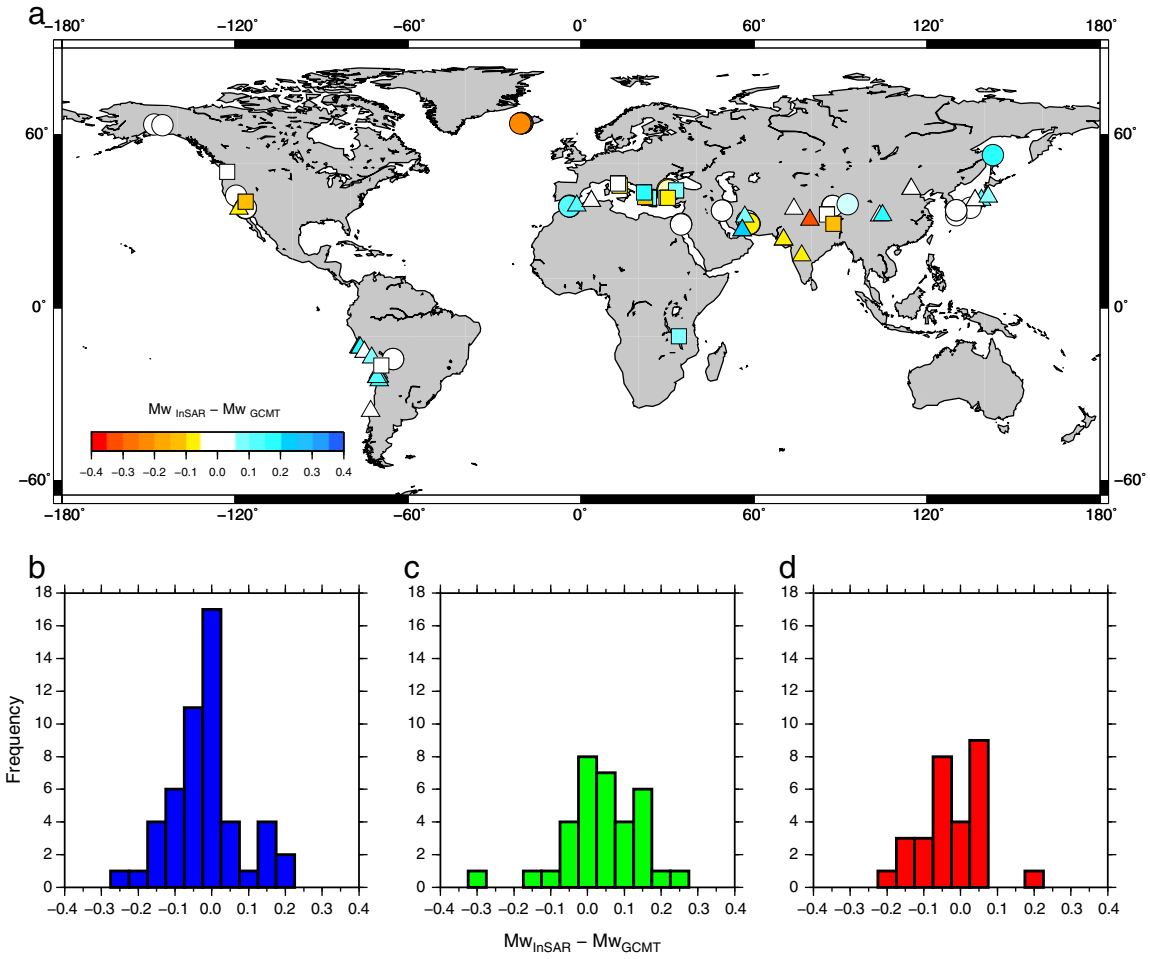

Fig. 2. a) Comparisons between InSAR and GCMT moment magnitudes with respect to fault mechanism and location, where circles, triangles and squares represent strike-slip, thrust and normal faulting events, respectively. b) Distribution of difference in moment magnitude for 51 strike-slip models, median = −0.02 (σ = 0.09). c) Same as in b) but for 34 thrust events, median = 0.04 (σ = 0.17) and d) 29 normal models, median = −0.03 (σ = 0.08).

is believed to be so high due to the large area affected by afterslip (Jouanne et al., 2011). Therefore, post-seismic deformation due to afterslip and viscoelastic relaxation appear to be the most likely physical mechanism to explain the larger moment magnitudes obtained using InSAR data for thrust earthquakes.

4.2. Earthquake location and source directivity

One of the key strengths of InSAR data is their high spatial resolution, so they can often be considered a 'ground-truth' for location estimates for moderate magnitude earthquakes. Comparisons with

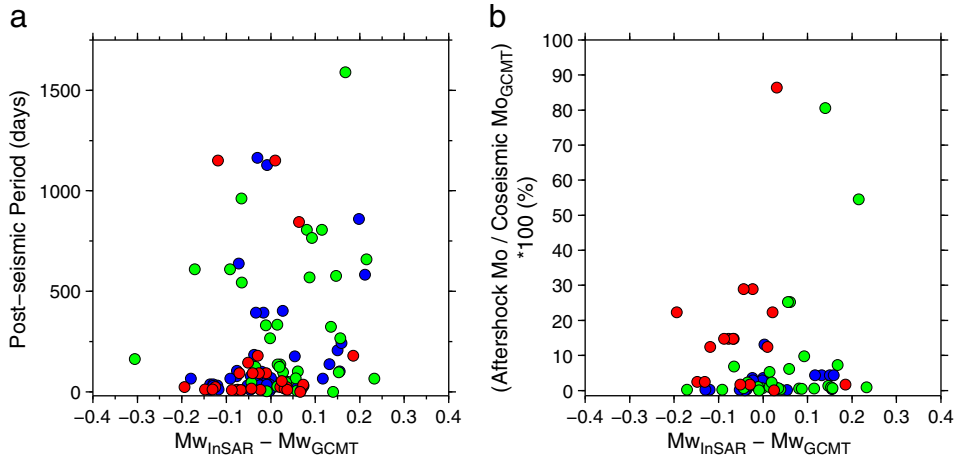

Fig. 3. Investigating the relationship between M_w, the post-seismic period and the total seismic moment contribution from aftershocks (see text for further explanation), with respect to faulting mechanism. There are 51 strike-slip models, 34 thrust and 29 normal faulting models represented by blue, green and red, respectively. a) The difference between InSAR and GCMT M_w estimates with respect to the post-seismic period. b) The difference between ICMT and GCMT M_w estimates with respect to the seismic moment release due to aftershocks as a fraction of the coseismic moment release reported in the GCMT catalogue.

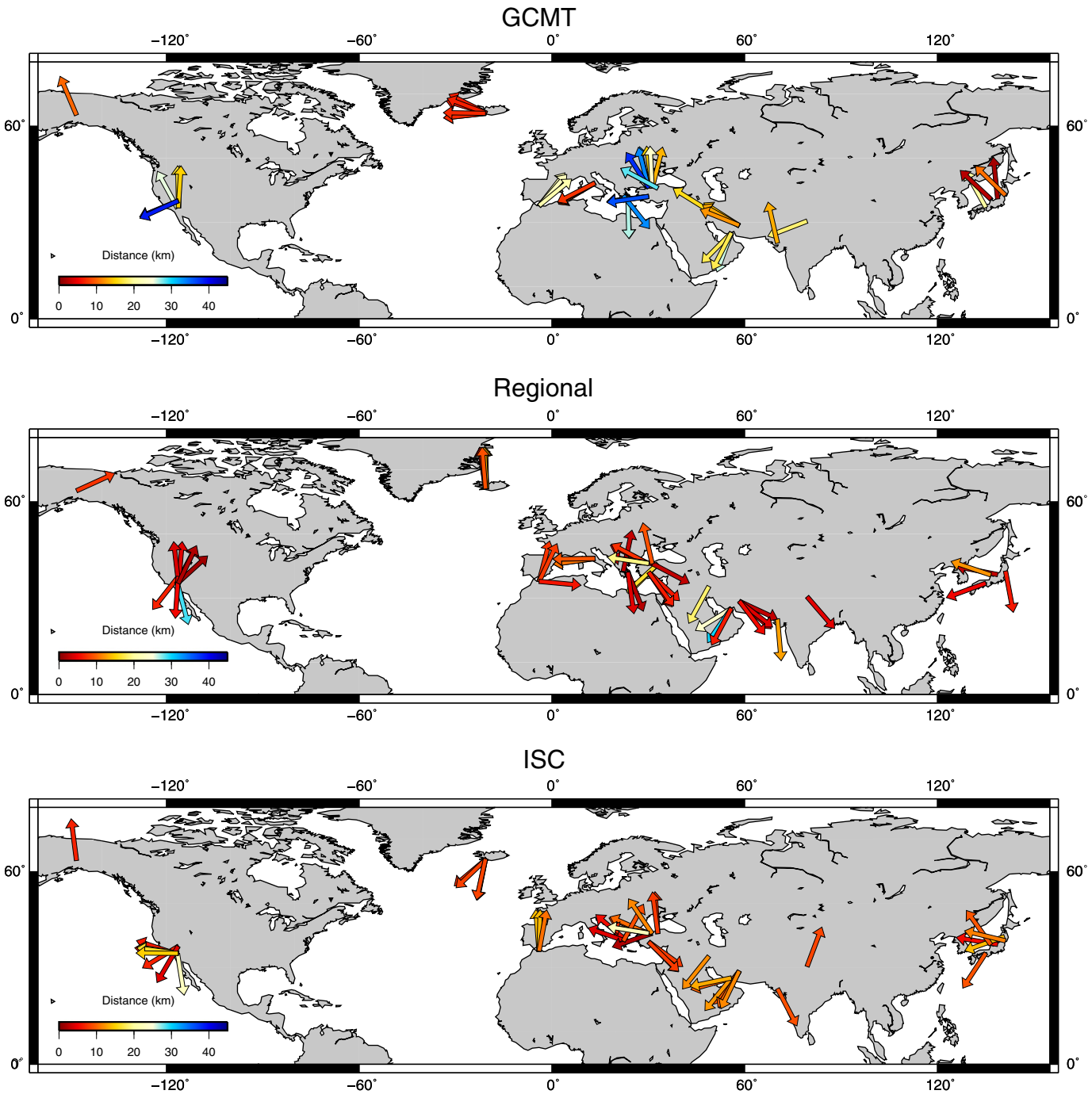

Fig. 4. Difference between InSAR centroid locations and 48 GCMT (Top) solutions, 50 regional seismic solutions (Middle; see also Section 2.2) and 46 ISC solutions (Bottom). The arrows are of constant size and are not to scale; they begin at the InSAR location and point in the direction of the seismic location where the distance in kilometres between the two locations is indicated by the colour of the arrow. The median difference for comparisons with GCMT is 16.96 km ($\sigma = 10.74$ km), for regional catalogues the median is 6.26 km ($\sigma = 6.49$ km), and a median of 9.23 km ($\sigma = 4.07$ km) is obtained for comparisons with the ISC catalogue. It must be noted that all comparisons in this figure are only for earthquakes with regional solutions.

seismic estimates using the updated database show the locations to differ by 21.0 km ($\sigma = 12.7$ km), 11.6 km ($\sigma = 6.9$ km) and 9.3 km ($\sigma = 7.5$ km) for GCMT centroid locations, and EHB and ISC hypocentre locations, respectively.

Generally, large disagreements are the result of poor quality InSAR data, showing for example decorrelation due to steep topography and possibly snow in the mountainous areas (e.g., for the Zarand earthquake, M_w 6.5, 22nd February 2005; Talebian et al., 2006). However, another cause of discrepancies is believed to be the use of simplified Earth models in seismic inversions. A good illustration of this is the systematic westward bias in locations of subduction zone earthquakes off the coast of South America by seismic catalogues (Pritchard et al., 2006; Weston et al., 2011). If the 3D variations in the velocity structure of subduction zones are taken into account when inverting seismic data, then the hypocentres can shift by up to 25 km (Syracuse and Abers, 2009).

Ferreira et al. (2011) found a similar trend for three events off the coast of Northern Chile in 1993, 1996 and 1998. Four different Earth models were tested and in some instances the disagreement between InSAR and CMT centroid locations was reduced by up to 40 km. Two

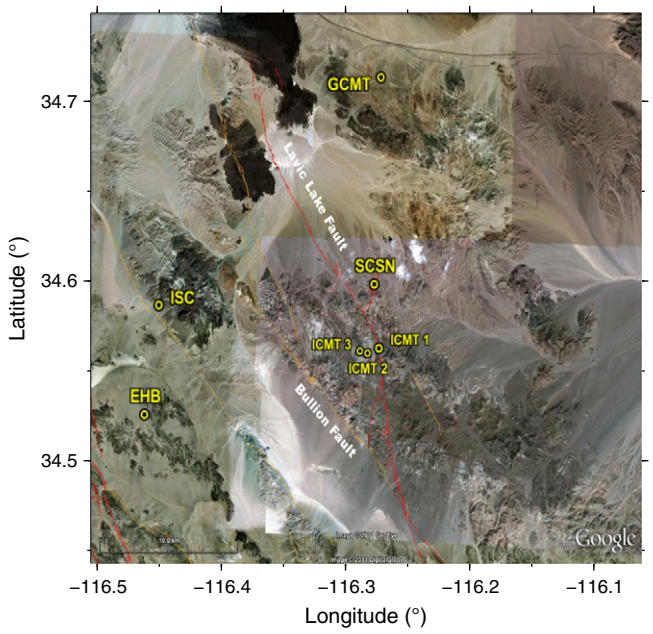

Fig. 5. Locations from InSAR and seismic data for the Hector Mine earthquake with respect to geological information. ICMT1 refers to the InSAR study Jonsson et al. (2002), ICMT2 refers to Salichon et al. (2004) and ICMT3 is Simons et al. (2002). SCSN is the hypocentre location from the SCSN catalogue. EHB, ISC and GCMT are the locations from these global catalogues. Mapped fault lines in red correspond to faults that have experienced movement in the past 150 years and the yellow lines are for faults younger than 15,000 years; they were plotted using Quaternary fault maps from the United States Geological Survey (California Geological Survey) (2006).

forward modelling techniques for the computation of synthetic seismograms were also considered but produced similar results for the same Earth model. However, these events were an isolated case and overall the use of different Earth models in the GCMT method did little to change the distances between the InSAR and GCMT centroid

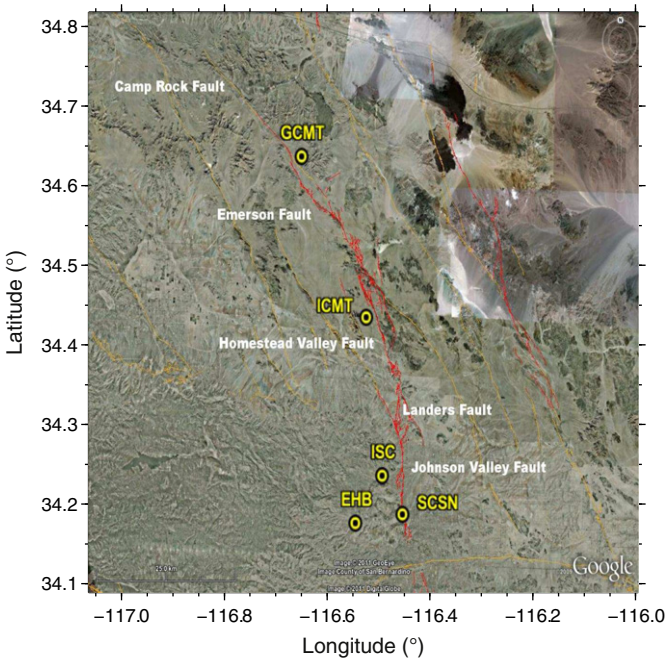

Fig. 6. Locations from InSAR and seismic data for the Landers earthquake with respect to geological information. ICMT refers to the InSAR study of Fialko (2004). SCSN is the hypocentre location reported in the SCSN catalogue. EHB, ISC and GCMT are the locations from the global catalogues. Mapped fault lines follow the same convention as in Fig. 5.

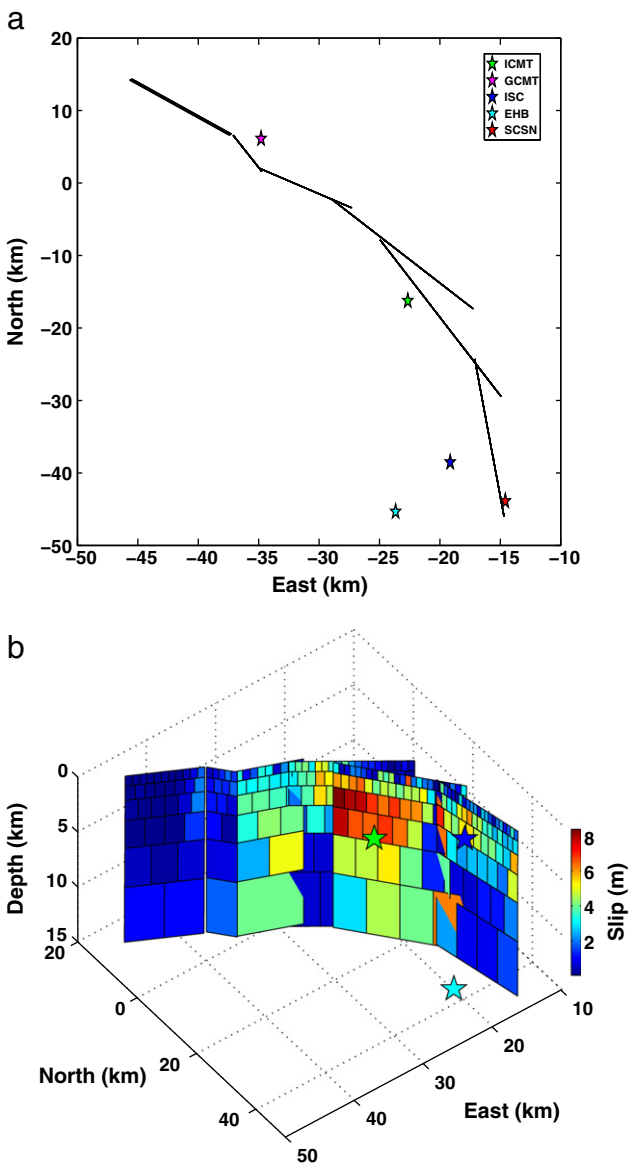

Fig. 7. Fault trace (a) and 3D view (b) of the subfaults used in the geodetic study of the Landers earthquake (Fialko, 2004), where the ICMT star indicates the centroid location for this model. The remaining stars are locations from the seismic catalogues described in the main text. Stars in (b) follow the same colour scheme as in (a).

locations. This suggests that for significant improvements in GCMT centroid locations higher resolution Earth models are needed (Ferreira et al., 2011).

In Fig. 4 location comparisons are carried out for earthquakes reported in regional catalogues (26 events). In general, for the moderate magnitude earthquakes considered in this study, there is better agreement between InSAR centroid location and seismic hypocentre locations from regional catalogues than for global catalogues, with a median difference of ~6.3 km compared with 9.2 km and 17.0 km for the ISC and GCMT catalogues respectively. As expected, this shows that the data from local networks used to determine the hypocentral locations reported in the regional catalogues can improve location determinations. Moreover, the local velocity models used in the inversions for the regional seismic catalogues further improve the accuracy of the locations.

Commonly, additional geological information can be used when determining a source model from InSAR or seismic data. When the fault ruptures up to the surface this provides a further constraint, and if mapped can then be used in the modelling process (e.g., Rigo

et al., 2004). Alternatively, slip measurements observed in the field (e.g., Hao et al., 2009) can be compared with displacements from InSAR data. Considering the fine spatial resolution of InSAR data, it is interesting to compare InSAR and seismically determined earthquake locations with the existing knowledge of geologically mapped surface offsets in an area. Here we focus on two events in Southern California; Hector Mine (M_w 7.1, 16th October 1999) and Landers (M_w 7.3, 28th June 1992). In Figs. 5 and 6, mapped locations of the faults known to have ruptured in the two earthquakes are compared with locations from seismic catalogues and InSAR studies. For Hector Mine (Fig. 5), the rupture initiated on a strand of the Lavic Lake fault, approximately at the SCSN location is, yet the EHB and ISC hypocentre locations are ~18 km to the west of this. A maximum right lateral slip of 5.25 m was observed 4 km south of the epicentre (Treiman et al., 2002), which agrees well with the InSAR centroid locations. The majority of the rupture occurred on the Lavic Lake fault as it propagated north-west, which may explain why the GCMT catalogue centroid estimate is 14–17 km north of the ICMT locations and ~9 km from the mapped Lavic Lake fault. Interestingly the ICMT locations are all on the west side of the mapped fault yet for two of the three InSAR solutions (Jonsson et al., 2002; Salichon et al., 2004) the fault dips to the east, in agreement with the solution in the GCMT catalogue. This issue and the slip distribution of the three InSAR solutions are discussed further in Section 5.1.

The Landers earthquake (Fig. 6) was larger than the Hector Mine event and involved five different faults with a total rupture length of ~80 km (Sieh et al., 1993). The agreement between the location of mapped faults and earthquake locations is better than for Hector Mine. The event is believed to have initiated on the Johnson Valley fault, as indicated by the SCSN location in Fig. 6, which also shows the ISC and EHB again to the west, by ~8 km. The GCMT is the most northerly location, slightly to the east of the Emerson fault, whereas the ICMT location (calculated from the InSAR model of Fialko (2004) is to the west of the fault zone near the central part of the Homestead Valley fault. This east–west difference in location is in agreement with the fact that the ICMT and GCMT solutions dip in opposite directions. Locations from the other three seismic catalogues suggest that the fault dips to the west rather than the east, in agreement with InSAR. Large offsets of more than 4 m were observed in the field on the Emerson fault in the north (Sieh et al., 1993) and slip distribution models from strong motion data showed more than 6 m of shallow slip on the Camp Rock and Emerson faults (e.g. Cohee and Beroza, 1994; Cotton and Campillo, 1995). However, probably due to these large surface displacements the interferograms are heavily decorrelated near the fault trace, so despite the use of azimuth offsets, the resulting slip distribution from these InSAR data appear to estimate much lower values of slip on the same faults. Consequently the maximum slip is nearer the middle of the rupture length in the InSAR derived finite fault model (Fig. 7) and the resulting ICMT centroid location is further south than the GCMT location. Furthermore, even though the GCMT location appears consistent with this maximum slip at the northern end of the rupture, ~50% of the moment is still estimated to have been released on the Homestead Valley fault (Cohee and Beroza, 1994). Therefore, errors in the assumed Earth model may also be affecting the GCMT location.

Despite this difference between the ICMT and GCMT centroid locations, when compared with hypocentre estimates from various seismic catalogues they both indicate rupture propagation towards the north. This is in agreement with rupture models calculated for this event (e.g. Cohee and Beroza, 1994; Wald and Heaton, 1994).

4.2.1. Source directivity

Comparisons of hypocentre and centroid locations can provide information regarding the rupture length and directivity. A previous comparison of ISC hypocentre locations and GCMT centroid locations showed that while for earthquakes with $M_w \geq 6.5$ these comparisons provide useful information, for smaller earthquakes the difference between the two can be heavily influenced by location errors, which are likely due to uncertainty in the assumed Earth models (Smith and Ekstrom, 1997). Taking this into account, Fig. 8 compares ISC hypocentre locations with GCMT and ICMT centroid locations for events with $M_w \geq 6.5$. It could be argued that for events larger than this, there are still significant errors associated with the locations reported in the GCMT and ISC catalogue (Weston et al., 2011). However, the hypocentre-centroid distances being considered here are on average larger than the errors previously found for ISC hypocentre locations; ~9 km in this study and ~3–16 km reported in (Syracuse and Abers, 2009). Also we are not using the differences between ISC and GCMT or ICMT locations as a means of definitively calculating the rupture length and direction, but rather to qualitatively investigate the consistency of results obtained using different centroid locations. Globally the distances between ISC hypocentres and ICMT and GCMT centroid locations are similar, with median distances of ~32 km and ~42 km, respectively. The orientations of hypocentre-centroid vectors show a mixed pattern globally (Fig. 8), where for some earthquakes there is good agreement with rupture directions from previous individual studies. For example, the Denali earthquake (M_w 7.9, 3rd November 2002) shows the largest difference between hypocentre and centroid location (~180 km), with the ICMT and GCMT centroids being in agreement with the unilateral south-east rupture models from various seismic and geodetic studies (e.g. Asano et al., 2005; Velasco et al., 2004). However, there are significant disagreements for several other events, as will now be discussed.

As one might expect from previous work (e.g. Weston et al., 2011), some earthquakes in the south American subduction zone show inconsistency between ICMT and GCMT centroid locations in relation to the ISC hypocentre. One of the largest discrepancies is in relation to three earthquakes in the northern Chile subduction zone; M_w 6.8, 11th July 1993, M_w 6.7, 19th April 1996, and M_w 7.1, 30th January 1998 (NC93, NC96 and, NC98 in Fig. 8c–d, respectively). The ICMT locations are relatively close to the hypocentre (4–13 km) whereas the GCMT locations are systematically located ~50 km to the west (Fig. 8c–d). As previously mentioned, this bias is thought to be the result of errors in assumed Earth models, so this systematic direction is unlikely to reflect the true rupture directivity.

In the same region there is also disagreement between ISC-ICMT and ISC-GCMT vectors for the Nazca Ridge earthquake (M_w 7.7, 12th November 1996, NR in Fig. 8c–d). The ICMT centroid location is twice as far away from the ISC hypocentre than the GCMT, but suggests a directivity in better agreement with the initial south east along-strike rupture propagation reported by Swenson and Beck (1999). It must be noted though that for the remaining earthquakes in this region there is general good agreement between reported rupture directivity and the ISC-ICMT and ISC-GCMT location vectors: Antofagasta (M_w 8.1, 30th July 1995, AN), Aiquile (M_w 6.5, 22nd May 1998, AI), Arequipa (M_w 8.1, 23rd June 2001, AR), Pisco (M_w 8.1, 15th August 2007, PI), and Tocopilla (M_w 7.8, 14th November 2007, TO).

The ISC-ICMT location vectors also appear to disagree significantly with the ISC-GCMT vectors for three events in the North Anatolian fault zone in Turkey. For example, if we consider these locations and a distributed slip model (Fig. 9) for the Izmit earthquake (M_w 7.5, 17th August 1999; Cakir et al., 2003) the GCMT centroid is a significant distance (~30 km) away from the modelled fault planes and when compared with the ISC and EHB hypocentres could imply a northward rupture propagation. However, the North Anatolian Fault on which this event occurred is not north–south trending and the InSAR-determined centroid locations (ICMT 1–3 in Fig. 9) are in better agreement with the observed surface geology and the modelled east–west bilateral rupture propagation from various seismic studies (e.g. Yagi and Kikuchi, 2000), particularly ICMT1 (Cakir et al., 2003) and ICMT2 (Wright, 2000) (Fig. 9). The ICMT3 (Delouis et al., 2002)

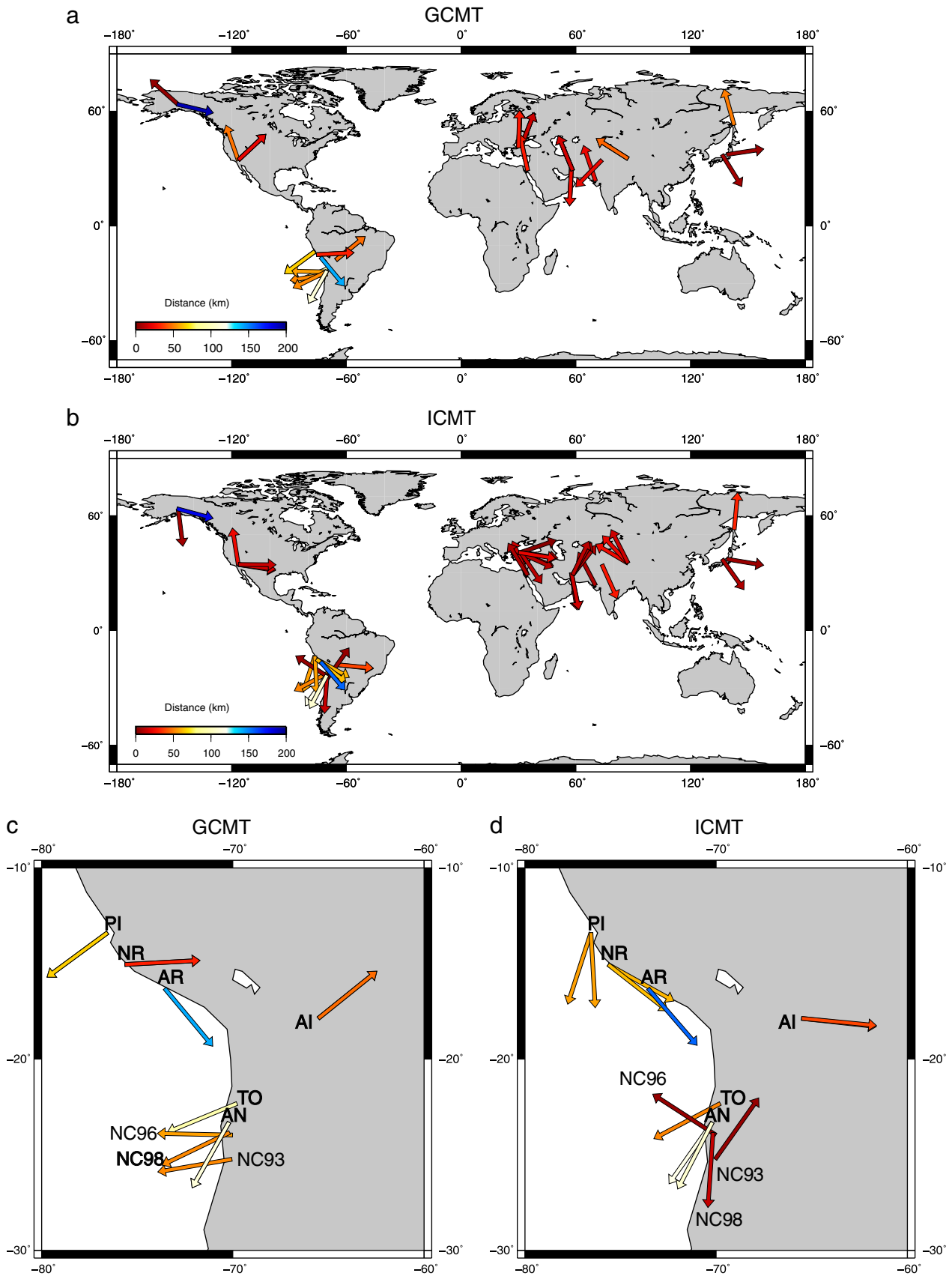

Fig. 8. Four maps illustrating comparisons between ISC hypocentre locations and GCMT centroid locations (a) and ICMT centroid locations (b) for 28 earthquakes; the ICMT comparisons have more arrows due to multiple InSAR studies for the same earthquake. All the arrows are the same size (not to real scale) and begin at the ISC location and point towards the centroid location where the colour of the arrow indicates the distance between the two locations. c) This is a zoomed-in map of ISC hypocentre and GCMT centroid locations for nine earthquakes in the South American region, d) is the same as c) except that it shows ICMT centroid locations instead. The labels next to each arrow refer to the name of the event where: AI = Aiquile, Bolivia; AN = Antofagasta, Chile; AR = Arequipa, Peru; NC93, NC96, NC98 = North Chile Subduction Zone 1993, 1996 and 1998, respectively; NR = Nazca Ridge, Peru; PI = Pisco, Peru, and TO = Tocopilla, Chile. See text for more details.

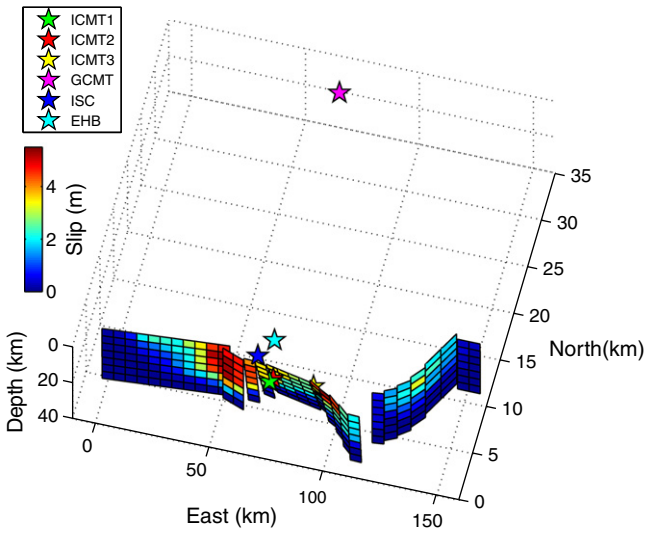

Fig. 9. Distributed slip model for the Izmit earthquake, from Cakir et al. (2003), where ICMT1 indicates the centroid location for this model. ICMT2 and ICMT3 refer to centroid locations from the studies of Wright (2000) and Delouis et al. (2002), respectively. The remaining locations are from seismic catalogues described in the main text (see figure legend).

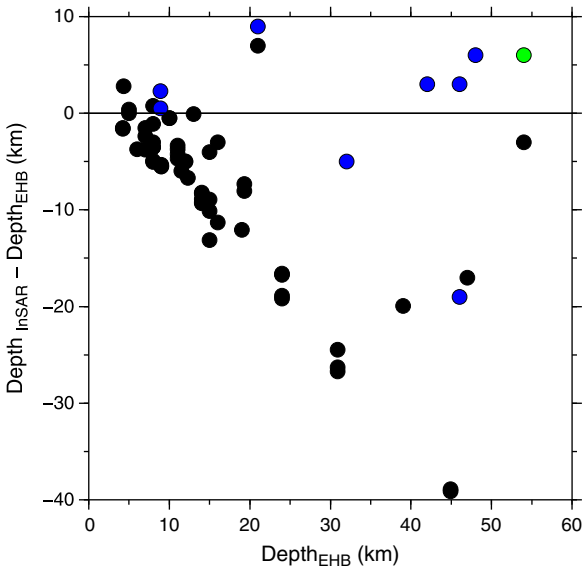

Fig. 10. A comparison of the differences in depth for parameters based on simple elastic homogeneous half-spaces (black circles), layered half-spaces (blue circles) and one 3D model (green circle).

location is from a distributed slip model that was calculated using GPS and seismic data as well as InSAR, which may explain the more easterly location.

Therefore, although centroid locations from InSAR derived variable slip models for large earthquakes can suffer the same issues as seismically determined locations when they are calculated from an inversion, they can provide valuable independent constraints on the spatial distribution of slip, which is useful for the determination of robust kinematic source models. Even without full kinematic spatiotemporal source inversions, the comparison of centroid locations obtained from InSAR slip models with hypocentre locations can also provide important information regarding rupture direction.

4.3. Depth

Accurate earthquake depth estimates can be difficult to obtain routinely for shallow crustal earthquakes. For example, the GCMT technique uses long-period body and surface waves, which cannot accurately determine depths in the upper crust of 15 km or less, thus the depth is often fixed at 12 km. Even the EHB catalogue, which has slightly better depth resolution (see Section 3.1), has to occasionally fix the source depth for earthquakes shallower than 12 km.

In contrast, InSAR source inversions commonly determine depths shallower than 12 km. It has been observed that InSAR depths are systematically shallower than those determined from seismic data (e.g., Lohman and Simons, 2005a; Weston et al., 2011). One reason for this is that the resolving power of InSAR data decreases with depth, which is evident from the diagonal trend of the data points in Fig. 10 showing that differences between InSAR centroid and EHB hypocentre depths increase with depth (this trend was also observed in Weston et al., 2011). The bias observed in this study is also consistent with observations of upward rupture propagation for shallow crustal earthquakes. Earthquakes that initiate in low stress regimes are thought to be unable to propagate deeper into a higher stress regime, if strength is assumed to increase with depth (Das and Scholz, 1983). Furthermore, InSAR data inversions usually assume elastic homogeneous half-spaces when modelling the surface deformation (see Section 2). Purely theoretical analyses (e.g., Cattin et al., 1999; Savage, 1987, 1998), investigations using geodetic data other than InSAR (e.g., Eberhart-Philips and Stuart, 1992; Hearn and Burgmann, 2005; Marshall et al., 1991; Wald and Graves, 2001), and results from inversions included in the database used in this review (Lohman and Simons, 2005a; Lohman et al., 2002) have found that depths determined assuming a homogeneous half-space are up to 30% shallower than those using layered Earth models. Feigl (2002) also suggests incomplete data coverage as a possible cause for the observed bias, a common issue for InSAR, and the fact that some events require a more complex solution than a planar fault. If a single planar fault with too shallow constant dip is used in the modelling process then it may not pass through the hypocentre, and the calculated depth will be shallower.

In recent years there have been some efforts towards the use of layered half-space models in the modelling of InSAR data and when this is considered the trend in depth comparisons between InSAR centroid depths and EHB hypocentre depths changes (Fig. 10). Despite the smaller dataset, centroid depths from InSAR studies that use layered half-space models appear to be in better agreement with the EHB hypocentre depths, with a median difference of 2.7 km ($\sigma = 8.7$ km) between the two types of estimates, compared with a median difference of −5.0 km ($\sigma = 9.2$ km) when using a homogeneous half-space in the modelling.

There are no evident relationships between faulting mechanism and differences in depth (Fig. 11). Also, there are no systematic trends in particular geographic regions probably because the events in the InSAR database were studied using a range of inversion methodologies and assumed elastic models to obtain the source parameters for events in a particular region. Not all of the studies in a region will have used the same homogenous or layered elastic half-space models. A more detailed investigation of regional trends requires source parameters determined using a uniform inversion technique and a consistent elastic model.

4.4. Fault geometry

Previously little attention has been paid to comparisons between strike, dip and rake fault values determined from the inversion of seismic and InSAR data. It is common for InSAR studies to use solutions from the GCMT catalogue or other seismic solutions as starting values for inversions (e.g., Baer et al., 2008), or even to fix the parameters at these values (e.g., Kontoes et al., 2000). Also, just by visually

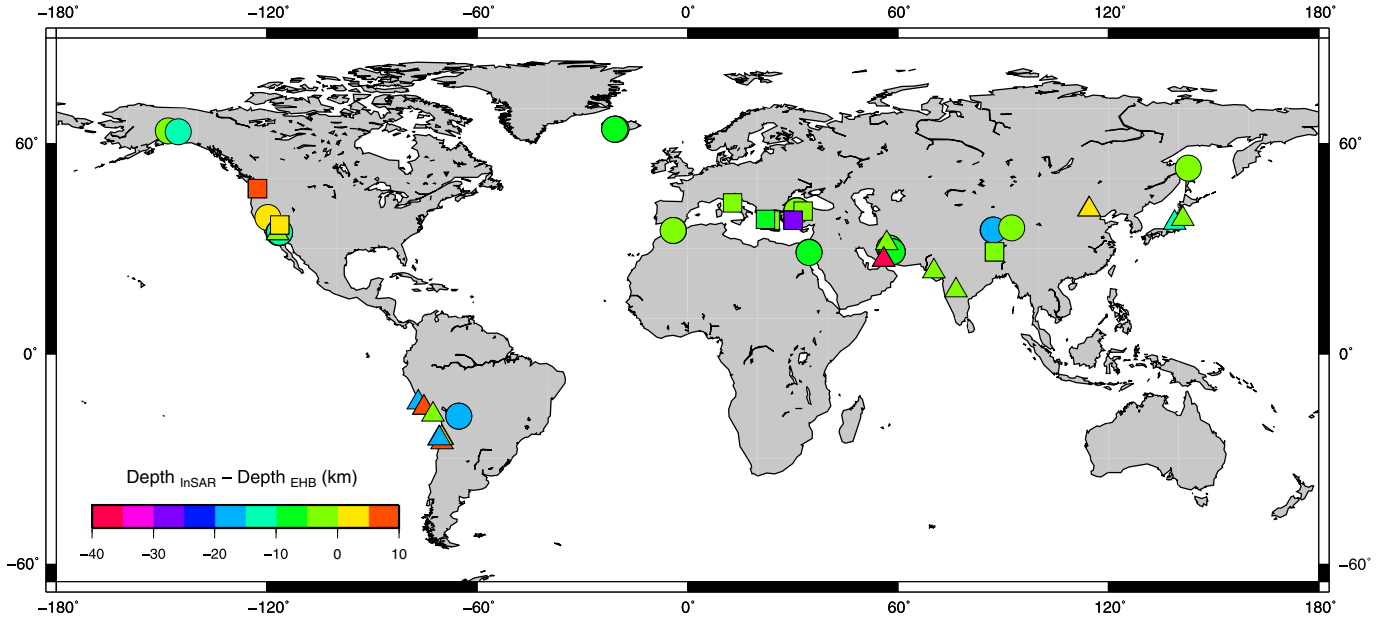

Fig. 11. Difference between InSAR centroid depths and EHB hypocentre depths with respect to mechanism and fault location, where circles represent 32 strike-slip models, triangles refer to 20 thrust models and 14 squares are normal faulting events. The median difference in depth is similar for all the mechanisms: −5.7 km, −2.7 km and −3.3 km for strike-slip, thrust and normal faulting, respectively.

examining an interferogram, significant constraints can be placed not only on the location but also on the orientation of the fault. This information can be used in the inversions as starting solutions or to fix the fault parameters to reduce the computational cost of the inversions (e.g., Funning et al., 2007; Jonsson et al., 2002).

We find here, as we did previously (Weston et al., 2011), that the strike, dip and rake values tend to agree well between InSAR and seismic models, the majority of the differences being within 20° (Fig. 12) and median values lying close to 0 for all parameters, 1.0°, (σ = 12.7°), 0.0° (σ = 14.6°), and −5.5° (σ = 16.4°) for strike, dip and rake, respectively. There are no clear trends when taking into account the faulting mechanism (Fig. 12). However, in some cases there are significant discrepancies for a variety of reasons, which will now be discussed.

Rake shows the widest distribution of differences between InSAR and GCMT solutions. This is largely due to the fact that when inverting InSAR data the rake is poorly constrained if only one track direction is used, as only a one dimensional measure of the deformation is available (e.g., Wright et al., 2004b). Therefore, it is difficult to distinguish between strike-slip and dip-slip motions, leading to poorly constrained rake values in the inversion. The −42° discrepancy in rake for Noto Hanto (M_w 6.7, 25th March 2007; Ozawa et al., 2008) is a good example of this, as only descending data from the ALOS satellite were used in the inversion with GPS data. However, Fukushima et al. (2008) used data from ascending and descending tracks for this same earthquake, and consequently this discrepancy in rake is reduced to 7° when compared with the GCMT solution.

Furthermore, since the image acquisition geometry of most SAR satellites leads to greater sensitivity to vertical than to horizontal motions, dip-slip motion is typically easier to detect using InSAR. Consequently the displacement seen in an interferogram could be due to a small dip-slip motion or equally due to a much larger strike-slip motion (assuming that the pattern of surface displacements is rendered sufficiently ambiguous by decorrelation or noise). Therefore, the seismic moment of an event can also vary greatly in an inversion, leading to a tradeoff between rake and moment and values related to seismic moment such as fault dip, slip, length and width (Funning, 2005). Inversions for the Ngamring County, Tibet earthquake (M_w 6.0, 20th March 1993; Funning, 2005) are a good example of these trade offs with a difference of 37.4° between the InSAR and GCMT rake values (Fig. 12). By inverting 100 datasets perturbed by random correlated noise with the characteristics of noise in the interferogram and examining the distribution of the model parameters thus obtained, Funning (2005) was able to identify which model parameters covaried. A significant tradeoff was found between rake and location in the inversion, as were dip-slip, slip-width, and dip-width tradeoffs.

These tradeoff issues can be further complicated by the presence of significant atmospheric and topographic effects. Poor data quality also affects other parameters, including strike; for example, the InSAR and GCMT strike solutions disagree by 39° for the Killari, India earthquake (M_w 6.1, 29th September 1993). The interferogram used suffers from significant temporal decorrelation due to land use changes and large areas of vegetation and surface water (Satyabala, 2006).

In addition, the way in which these comparisons have been conducted must be taken into consideration as only solutions from one seismic catalogue are used, but there may be several other published independent seismic solutions, which can differ greatly from the GCMT solutions. For example, even though there is a 34° discrepancy in strike for the Qeshm Island event (M_w 5.8, 28th June 2006) the difference between the study's InSAR solution and their own seismic solution from the inversion of body wave data is reduced by half, to a difference of 17° (Nissen et al., 2007).

A further difference that is an artefact of the method of comparisons is the 46° discrepancy in strike between the InSAR and GCMT estimate for the Al Hoceima earthquake (M_w, 24th February 2004, Tahayt et al., 2009). The InSAR solution is a cross-fault model (i.e., with two conjugate fault planes that both slipped in the event) and a moment-weighted average strike of the two faults (Weston et al., 2011) has been used for comparisons. Thus, such an average is not a true representation of the source and not a fair comparison with the GCMT solution, which is a simple point source solution.

Overall strike, dip and rake agree well between InSAR and seismic solutions and this is evident from Fig. 13, where circles, triangles and squares represent strike-slip, thrust and normal faulting mechanisms,

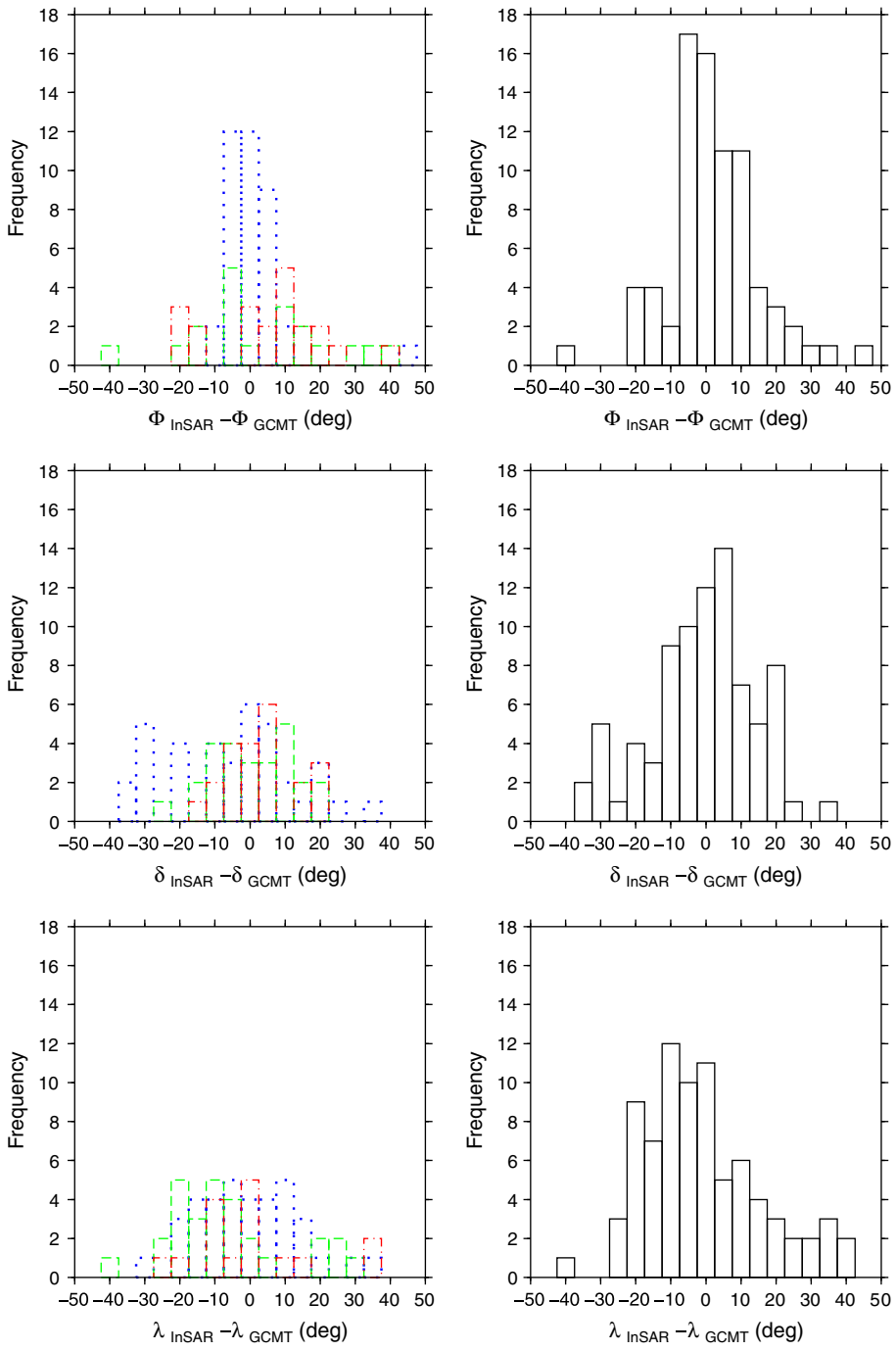

Fig. 12. Comparison of InSAR and GCMT strike, ψ (top), dip, δ (middle) and rake, λ (bottom). The diagrams show the distribution of the difference with respect to mechanism, where the blue dotted line corresponds to strike-slip, green dash is thrust and red dash dot refers to normal faulting events (see text for details). The figures on the right side are the total distribution of all the mechanisms, for 78, 85 and 80 estimates of strike, dip and rake, respectively, where the median and standard deviations for each of the parameters is as follows; $\psi = 1.0°$, ($\sigma = 12.7°$), $\delta = 0.0°$ ($\sigma = 14.6°$), and $\lambda = -5.5°$ ($\sigma = 16.4°$).

respectively. There are no clear patterns in terms of the geographical distribution of the differences in fault strike, dip and rake suggesting that InSAR and seismic data constrain the fault geometry equally well and are relatively insensitive to the Earth models assumed in the inversion of seismic data and the elastic models used to model InSAR data. However, similar to the depth comparisons (Section 4.3), the lack of regional trends could alternatively be due to the use of different inversion techniques and Earth structure models for events in the same region. This highlights the importance of taking the inversion technique and assumed Earth model into account when comparing different source models for the same event.

5. Distributed slip models

5.1. Intraevent variability

During the past three decades there have been several notable earthquakes that have been studied independently by multiple groups using InSAR data. A good example of this is the M_w 7.1 Hector Mine earthquake, previously discussed in Section 4.2. Fig. 14 shows three distributed slip models for this event, produced using InSAR data. Models a (Jonsson et al., 2002) and b (Salichon et al., 2004) have been built using the same InSAR data from ascending and descending tracks from the

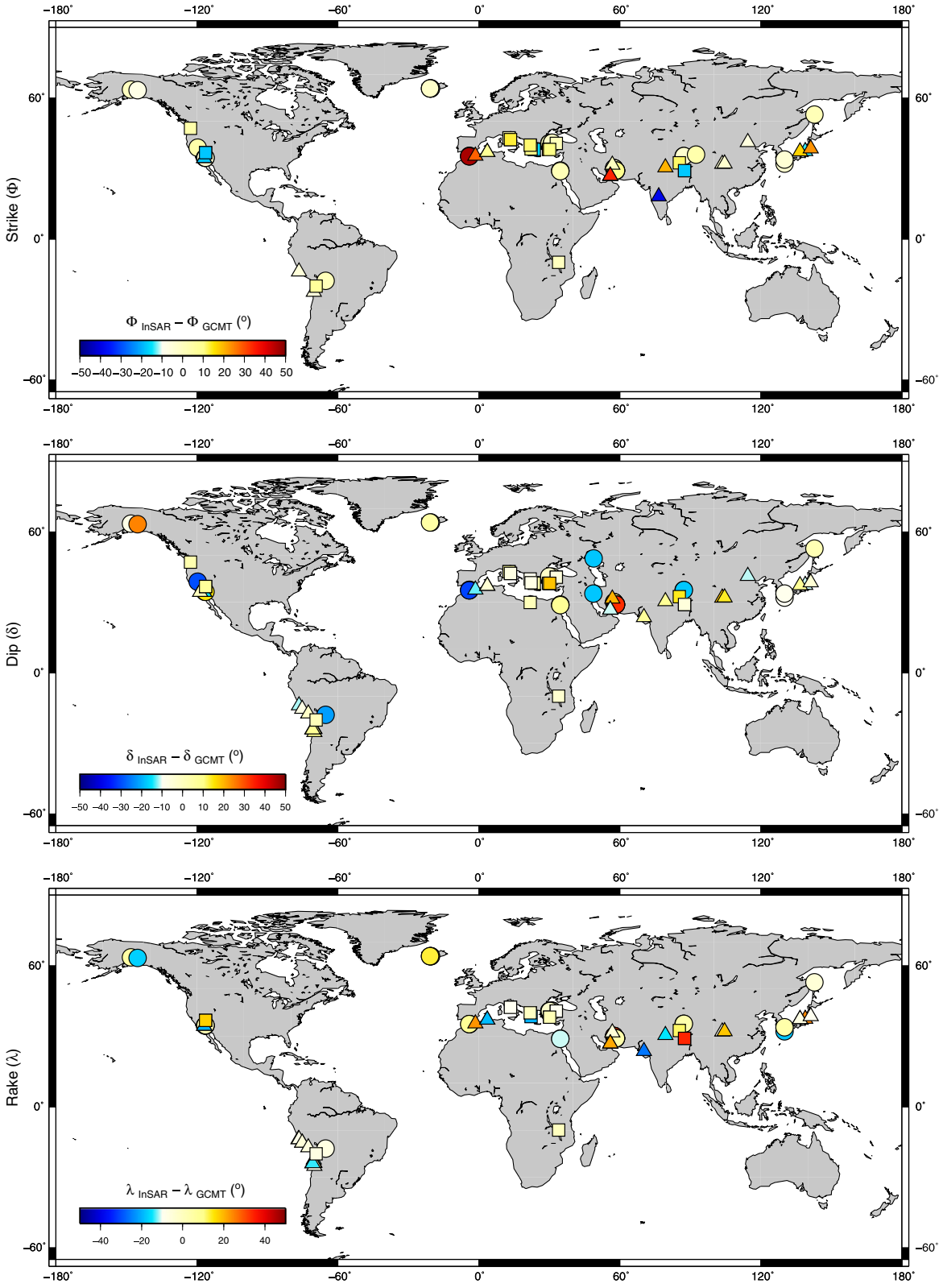

Fig. 13. Differences, in degrees, between GCMT and InSAR strike, dip and rake with respect to mechanism and InSAR location. The notation for each mechanism is the same as in previous figures (strike-slip = circle, triangle = thrust, square = normal).

ERS-1 andERS-2 satellites, to produce interferograms with measurement periods of 35 days. Model c (Fig. 11c, Simons et al., 2002), uses an ascending interferogram covering a longer period of ~4 years. The fault geometry is complex for this event and each study uses multiple fault segments, varying from 4 to 9. Despite the varying numbers of segments, the length, width, strike and rake values are consistent across all the models, likely the result of the fact that the trace of the surface rupture is well constrained by the InSAR data.

However, there is some discrepancy in the direction of dip, as mentioned in Section 4.2. For the ICMT models a and b, and the

GCMT solution, the fault is dipping to the west whereas the fault segments dip eastwards in model c. It must be noted though that when solving for the slip distribution the dip was held fixed in models a and b. The difference in dip is small because it is near vertical for all models (dip = ~82°). The principal difference between model c and the other two is that Simons et al. (2002) use a layered half-space, which could be responsible for the variation in dip direction.

As discussed in Section 4.3, the use of a layered half-space can reduce the bias towards shallower depths seen in InSAR models that use a homogeneous half-space. Yet even though the peak slip is in the north-west part of the rupture for models a–c, it is shallowest in model c. Therefore different methods of inversion and model parameterisations could be responsible for the variation in dip and the depth of maximum slip. Furthermore, only one of the interferograms used by Jonsson et al. (2002) includes post-seismic deformation due to afterslip in the month following the earthquake. In comparison, both the ascending and descending tracks used in Simons et al. (2002) could include post-seismic deformation, which could also explain why their estimated geodetic moment is the largest of the three models (~20% larger than models a and b).

The slip distribution in model b extends ~12 km further to the south-west than the other two models, which could be a result of the inclusion of teleseismic data in the inversion, although little change in the spatial pattern of the slip distribution was seen when these additional data were included (Salichon et al., 2004). Very similar InSAR datasets are used in each of the three studies, consequently the variations in the slip distribution models are most likely the result of differences in inversion methods. The relative weighting of the InSAR, GPS and seismic datasets used is of particular importance because it dictates the influence each dataset has on the final inversion result, an issue discussed in Section 6.3, as well as *a priori* constraints such as model regularisation (smoothing).

5.2. Earthquake location

As mentioned previously, one of the strengths of InSAR data is their spatial resolution, where visual examination of the interferogram can place strong constraints on the location of an earthquake. However, for large magnitude events with long rupture lengths the InSAR-determined centroid location is calculated from a slip distribution, which is the result of an inversion, and consequently suffers from similar issues as seismically determined locations that are also determined from an inversion. Here we illustrate differences in location between seismic and InSAR (distributed slip) determinations for the Wenchuan earthquake (M_w 7.9, 12th May 2008). This large, predominantly, thrust event occurred in the Longmen Shan range and was one of the largest intraplate events in recent years, with a very complicated surface rupture that sparked many seismological, geodetic and fieldwork studies (e.g., Ghasemi et al., 2010; Li et al., 2010; Liu-Zeng et al., 2010; Zhang and Ge, 2010).

The rupture initiated near Wenchuan and propagated unilaterally to the north-east (e.g., Zhang and Ge, 2010), which is consistent with the NEIC hypocentre estimate (blue star in Fig. 15) in relation to all the calculated centroid locations (pink star, GCMT location; green, Hao et al., 2009, and yellow, Feng et al., 2010). There is a significant offset between the GCMT centroid location and the two estimates from InSAR studies; 38 km and 28 km for Hao et al. (2009) and Feng et al. (2010), respectively. However, considering the large magnitude of this event and compared with the previous case studies (Landers, Hector Mine and Izmit in Section 4.2), the two InSAR

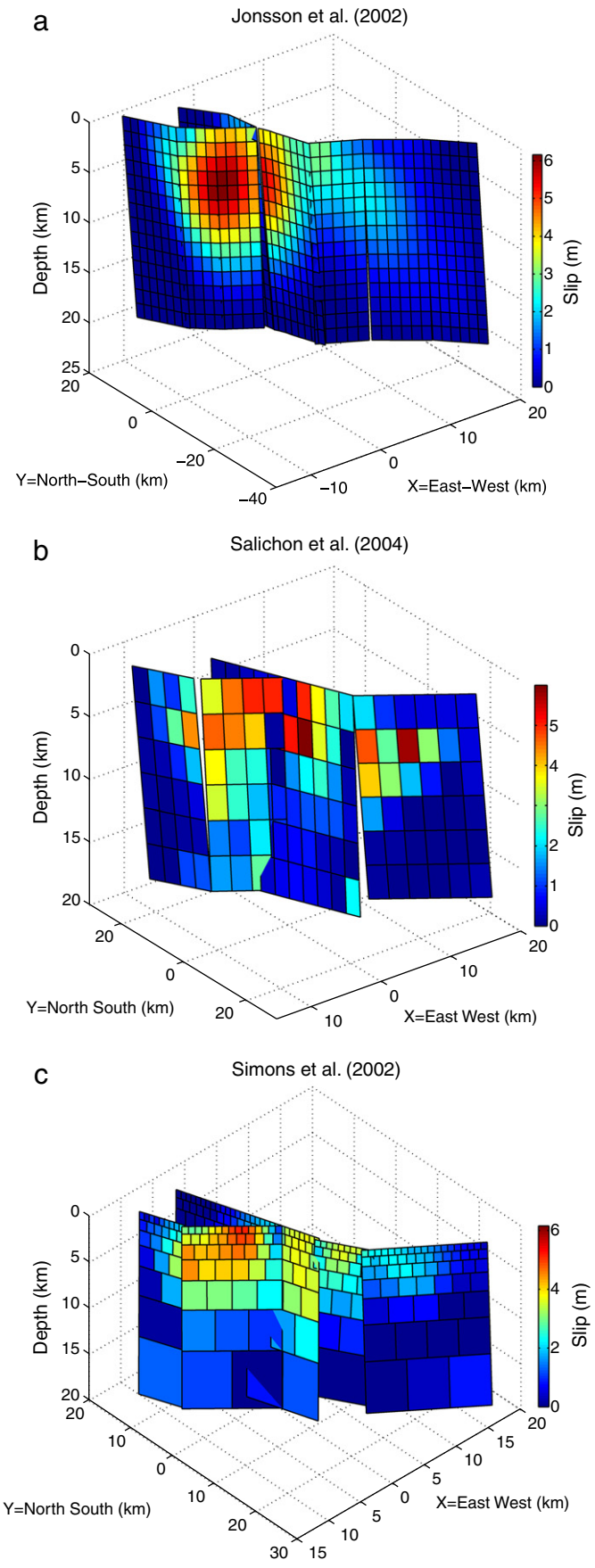

Fig. 14. Comparison of three distributed slip models for the Hector Mine earthquake (M_w 7.1, 16/10/99). a) Jonsson et al. (2002), which results from the joint inversion of InSAR and GPS data, b) Salichon et al. (2004), which jointly inverted InSAR, GPS and teleseismic data and c) Simons et al. (2002), which results from the joint inversion of InSAR and GPS data.

estimates are in good agreement with each other (~22 km), and the differences seen are likely due to some discrepancies in the slip distribution. In particular the maximum slip is much lower in the model from Feng et al. (2010) (Fig. 15b) ~7 m, compared with ~12 m for Hao et al. (2009). The latter study also obtains a larger area of higher slip for the hypocentre at the south-west end of the rupture. Both models use similar InSAR data (ALOS data from tracks 471–477), but Hao et al. (2009) use measurements of offset observed in the field to help constrain the source model, whereas GPS and InSAR data were used in Feng et al. (2010), which may explain the observed difference.

There are also large variations in the finite fault models for this event that are calculated using seismic data (e.g., Ji and Hayes, 2008; Liu-Zeng et al., 2009). Generally both geodetically and seismically determined source models appear to model two large asperities, one near the hypocentre and one ~150 km to the north east ,but the asperity areas and magnitude of slip vary substantially between them. The two InSAR source models have one or two more subfaults than are used in the seismically derived source models (e.g. Ji and Hayes, 2008) which are in agreement with observed surface ruptures (e.g. Liu-Zeng et al., 2009). The source model from Hao et al. (2009) is more consistent with the high peak slip seen in the seismically derived source models and offsets observed in the field (e.g. Liu-Zeng et al., 2009; Nakamura et al., 2010). The large number of varying finite fault models that fit the observed data is potentially due to the complicated nature of the rupture. Despite this complexity, the relative good agreement in centroid location between the two InSAR studies demonstrates the ability of InSAR to constrain the spatial features of the rupture.

6. Discussion and conclusions

6.1. Source parameter validation

Seismic and InSAR data are independent observations of different aspects of an earthquake, therefore with our compilation of source parameters from published InSAR studies, it is possible to validate source parameters from seismic catalogues against an independent dataset. Comparisons between databases compiled using InSAR and seismic catalogues have highlighted certain issues. For example, the comparisons of GCMT and InSAR centroid locations have highlighted limitations in the GCMT location, as well as the influence that the Earth model used in CMT inversions has on the location of the events (Ferreira et al., 2011). Conversely, the good agreement between strike, dip and rake values suggests how well both datasets constrain these particular parameters.

Comparisons between InSAR and seismic data can be used to quantify uncertainties in source parameters reported in seismic catalogues or InSAR studies. For example, as previously mentioned, the location from the GCMT catalogue varies on average by about 21 km from the InSAR centroid location (Weston et al., 2011). The moment magnitude differs by ~0.01 ($\sigma = 0.10$) and fault geometry estimates (strike, dip and rake) by ~0°–5° ($\sigma = 13°–16°$). The standard deviations also give an idea of the level of uncertainty associated with the source parameters determined using various inversion techniques with seismic and geodetic data. These uncertainties need to be taken into account when using earthquake source parameters to determine for example changes in tectonic stress (e.g., Coulomb stress changes; King et al., 1994) in an area, as these are sensitive to

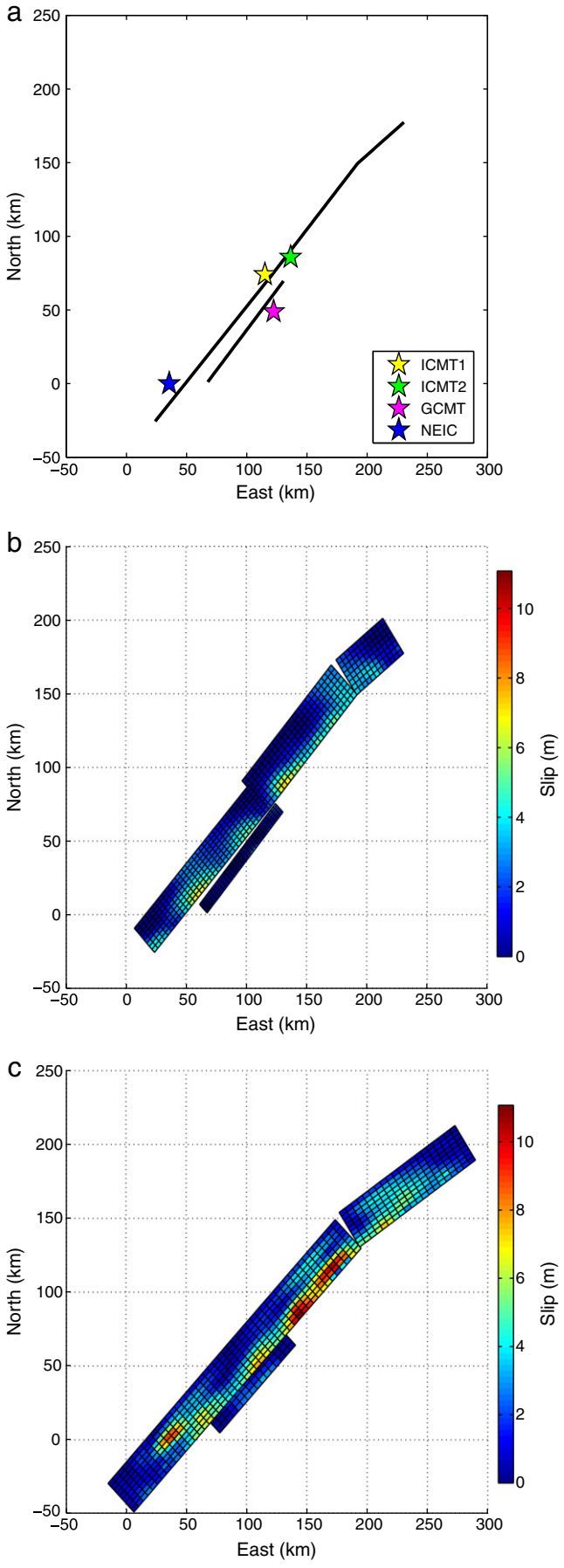

Fig. 15. a) Fault trace of the distributed slip model for the Wenchuan earthquake from Feng et al. (2010), where ICMT1 refers to the centroid location from the same study, ICMT2 is the centroid location from Hao et al. (2009), GCMT is the centroid location reported in the GCMT catalogue and NEIC is the hypocenter location from the NEIC Preliminary Determination of Epicenters (PDE) catalogue. b) Plan view of the Feng et al. (2010) distributed slip model. c) Plan view of the Hao et al. (2009) distributed slip model.

fault orientation, which in turn can be used for assessing seismic hazard.

6.2. Spatial and temporal resolution

InSAR and seismic data are contrasting datasets regarding their spatial and temporal resolution. InSAR can be seen as a 'ground truth' for the location of moderate magnitude earthquakes, but lacks temporal resolution. In interferograms that span a long time interval, deformation from events other than the earthquake that occur in this period can have a strong influence on the quality of the interferogram (see Section 4.1) and consequently on the models obtained from the inversion of these data. The influence of atmospheric perturbations is also a key issue, and methods for characterising and removing these are currently being developed (see Section 2.1). The effects of post-seismic deformation would be reduced by using interferograms where the post-event image was acquired as quickly as possible after the earthquake, currently an unlikely scenario given the long repeat interval between satellite passes for most missions. When the SENTINEL satellite is launched in 2013, it will have a repeat orbit of 12 days; once the second satellite is available, the time period between images on the same track could be reduced to just six days (Potin, 2011), compared with 35 days for the majority of the ERS-1 and ERS-2 missions and the Envisat mission.

In comparison, seismic data have much better temporal resolution than InSAR, which in turn have often better spatial resolution and accuracy; therefore, these two datasets are very complementary. InSAR and seismic data are both powerful tools for constraining the slip distribution; yet, when combined, the InSAR data can further refine the spatial distribution of slip and seismic data are able to constrain the temporal features (e.g., Salichon et al., 2004).

6.3. Joint inversions

It has already been highlighted how the relative strengths of InSAR and seismic data regarding spatial and temporal resolution complement each other in joint source inversions. Increasingly, InSAR data are being jointly inverted with other types of data, particularly GPS and seismic data. All these datasets can introduce tradeoffs, particularly for dip, rake and moment but, when combined, these tradeoffs can be reduced (e.g., Atzori et al., 2009; Funning, 2005).

There are various approaches to weighting the contribution of each dataset in the inversion, which are well summarised in Sudhaus and Jonsson (2009). The weights can be equal (e.g., Belabbes et al., 2009b) or arbitrary weights can be set (e.g., Delouis et al., 2002). The weights can be based on misfit statistics (e.g., Salichon et al., 2004) or the covariance of each dataset (e.g. Sudhaus and Jonsson, 2009; Wright et al., 2004a). Alternatively, the datasets can be normalised so that the sum of the weights assigned to the individual data points is equal to one and consequently the weights are inversely proportional to the measurement errors (e.g., Fialko, 2004). A similar approach can be taken if the data are subsampled, and in this case the weights can be related to the area that each of the data points represent (e.g., Simons et al., 2002).

6.4. Estimation of uncertainties

The estimation of uncertainties is an area of increasing focus concerning radar interferometry, as initially the errors involved with InSAR data were not fully understood, likely the result of the numerous contributing factors of uncertainty that have to be accounted for. Incomplete data or errors in the data itself, the properties of the elastic medium and other assumptions made in the modelling process can all introduce uncertainties. Furthermore, as there is no uniform method for processing and modelling InSAR data, a blanket approach to assessing the uncertainty cannot be used (Sudhaus and Jonsson, 2009).

There are various methods of quantifying the effects of errors in the data, one example being to add representative noise to the interferogram and observing the tradeoffs and uncertainties in source parameters determined from these 'noisy' datasets (e.g., Wright et al., 2003). Noise, being the effect of differences in water vapour content in the troposphere, or of charged particles in the ionosphere between the two SAR acquisition dates, is typically spatially correlated. Thus, to accurately simulate the noise in an interferogram, it is important to accurately estimate the length scale over which it is correlated (e.g., Lohman and Simons, 2005a). Following a similar approach, Dawson and Tregoning (2007) calculated synthetic interferograms for 84 (M_w 2.4–6.7) intraplate earthquakes in Australia and perturbed them with characteristic noise. These simulated 'noisy' interferograms were then inverted for source parameters which were compared with the original parameters used to produce the simulated interferograms. For earthquakes greater than M_w 5.8 the horizontal component of the epicentral location could be determined to within 0.07 km, the depth within 0.15 km and the strike 0.2°, whereas for smaller events (M_w 5.5) this uncertainty increases to 0.3 km, 0.5 km, and 1.0°, respectively. If we consider the different models for individual events in this study the variability in parameters appears larger than these values; for example strike angle can vary between 1 and 10°, depth by 1–4 km and location by 2–12 km. This suggests that although noise is a key consideration it is not the most important factor which influences the variability of the inversion solutions; the different methods and assumed earth models used are also highly influential. Furthermore, noise-related variability is a random error, whereas Earth model variability can result in systematic errors which are harder to detect and quantify.

The accurate determination and use of uncertainty in the data is key for joint inversions that weight the data based on these errors. An approach by Sudhaus and Jonsson (2009) incorporates the error characteristics of the InSAR data by using the inverse of the data covariance matrix to weight data points so that poorly constrained or highly correlated data points are given less weight and vice versa. The covariance matrix can also be used to propagate the data uncertainties through the model to obtain source parameter uncertainties. Despite the various methods becoming available it is still not routine in studies to report the errors in earthquake source parameters.

6.5. Earth models

Source parameters, whether they are obtained by inverting seismic or InSAR data, are sensitive to the assumed Earth model used to compute synthetic seismograms or synthetic line-of-sight displacements, respectively. Ferreira and Woodhouse (2006) were the first to attempt to quantify the uncertainties in seismic CMT inversions due to inaccurate Earth structure using a variety of Earth models and forward modelling techniques. The global Earth models used in global seismic catalogues currently do not seem to have high enough resolution to accurately locate shallow crustal events (Ferreira et al., 2011). Mellors et al. (2004) also found the Earth model, in this case regional rather than global, to be an influential factor when comparing InSAR and seismic source parameters. The InSAR derived source parameters agreed well with those determined from seismic data relocated using a 3D velocity model, but the agreement was poorer with seismic parameters obtained employing 1D velocity models.

The assumption of a homogeneous half-space in InSAR data inversions leads to a bias toward shallower depths, but even though a layered half-space is an improvement, it does not solve the problem. The layered or 3D earth model must be accurate, as found by Cattin et al. (1999), who investigated the effect of the inclusion of a lower rigidity layer in a homogeneous half-space on modelled coseismic surface displacements and the interpretation of source parameters. The horizontal component of displacement was more sensitive than the vertical

component to the inclusion of the layer. Horizontal displacements could increase by up to 40% using a half-space that incorporates a lower rigidity layer at the surface in comparison with motions determined using a homogenous half-space. If InSAR data from only one SAR track direction are available, then horizontal motions (particularly those in the north–south direction) are already poorly constrained with respect to the vertical component; if in addition the Earth model is incorrect, further errors are introduced.

The Earth model used for inversion of both sets of data is clearly a key consideration for the calculation of robust source parameters, particularly location and depth. However, comparisons between the two types of Earth model used by each dataset are hard to make due to the large difference in scale. For long-period seismic data improvements in Earth models on a continental scale are needed whereas local-scale structural improvements would be more beneficial for inversions using InSAR data. Also when comparing InSAR and seismically determined locations, the effect of the Earth model on seismic locations is more important than the equivalent effect on InSAR locations. Varying the Earth model in seismology can result in changes in location of tens of kilometres laterally and a few kilometres vertically (e.g., Engdahl et al., 1998; Smith and Ekstrom, 1996; Syracuse and Abers, 2009), whereas for geodetic data depth-dependent changes in elastic structure result in smaller variations in location laterally and vertically (e.g., Bustin et al., 2004; Hearn and Burgmann, 2005). Currently the InSAR locations have smaller Earth model-related uncertainties, and thus provide more robust locations than long-period seismic data. Detailed study of the differences between the locations provided by the two techniques could thus provide a novel means of identifying errors in current seismic Earth models in future.

6.6. Conclusions

Since the first InSAR study of an earthquake (Landers, M_w 7.3, 28th June 1992, Massonnet et al., 1993) the interest in the technique has grown and its valuable contribution towards the calculation of robust source parameters is now recognised, illustrated by the continued and future investment in satellites used for data acquisition.

Overall, InSAR and seismic data lead to seismic source parameters that agree well concerning the fault geometry and are complementary datasets when jointly inverted. The assumed Earth structure model is an influential factor concerning the quality of the earthquake location and depth. Seismic locations from regional catalogues show the best agreement with InSAR locations, relative to those from global seismic catalogues. Centroid locations from InSAR slip models when compared with hypocentre locations can also provide important information regarding rupture directivity. In terms of the moment magnitude, there is generally good agreement, with a tendency for the InSAR estimates for thrust events to be slightly larger. This is a possible artefact of the events included in the study and also the result of potential deformation from aftershocks, afterslip and viscoelastic relaxation being included in the measurement period, and increased sensitivity to vertical motion. Techniques for the processing and inversion of both InSAR and seismic data are constantly being refined, however particular focus is needed on verifying the accuracy of the assumed Earth model and the accurate quantification of uncertainties.

Acknowledgements

Thank you to all the authors who responded to the requests for variable slip models, see list in Weston et al. (2011) and we would also like to thank the following authors who provided the additional variable slip models used in this study: Simone Atzori, Eric Hetland, Ken Hao, and Mahdi Motagh. Thank you to H. Bloomfield for her help with the variable slip models plotted in this study. Also thank you to the anonymous reviewer for their comments, which helped improve the quality of the manuscript. The research presented in this paper was carried out on the High Performance Computing Cluster supported by the Research and Specialist Computing Support services at the University of East Anglia. JW is funded by NERC. AMGF is grateful to support from the European Commission's Initial Training Network project QUEST (contract FP7-PEOPLE-ITN-2008-238007).

References

Adams, R.D., Hughes, A.A., McGregor, D.M., 1982. Analysis procedures at the International Seismological Centre. Physics of the Earth and Planetary Interiors 30, 85–93.
ANSS, 2010. Earthquake Catalog Details. http://www.ncedc.org/anss/anss-detail.htmlcatalog-creation, 2010, Last Accessed 01/05/2011.
Asano, K., Iwata, T., Irikura, K., 2005. Estimation of source rupture process and strong ground motion simulation of the 2002 Denali, Alaska, Earthquake. Bulletin of the Seismological Society of America 95, 1701–1715.
Atzori, S., Hunstad, I., Chini, M., Salvi, S., Tolomei, C., Bignami, C., Stramondo, S., Trasatti, E., Antonioli, A., Boschi, E., 2009. Finite fault inversion of DInSAR coseismic displacement of the 2009 L'Aquila earthquake (Central Italy). Geophysical Research Letters 36, L15305.
Baer, G., Funning, G.J., Shamir, G., Wright, T.J., 2008. The 1995 November 22, Mw 7.2 Gulf of Elat earthquake cycle revisited. Geophysical Journal International 175, 1040–1054.
Belabbes, S., Meghraoui, M., Cakir, Z., Bouhadad, Y., 2009a. InSAR analysis of a blind thrust rupture and related active folding: the 1999 Ain Temouchent earthquake (Mw 5.7, Algeria) case study. Journal of Seismology 13, 421–432.
Belabbes, S., Wicks, C., Cakir, Z., Meghraoui, M., 2009b. Rupture parameters of the 2003 Zemmouri (Mw 6.8), Algeria, earthquake from joint inversion of interferometric synthetic aperture radar, coastal uplift, and GPS. Journal of Geophysical Research 114, B03406.
Biggs, J., Bergman, E., Emmerson, B., Funning, G.J., Jackson, J., Parsons, B., Wright, T.J., 2006. Fault identification for buried strike-slip earthquakes using InSAR: the 1994 and 2004 Al Hoceima, Morocco earthquakes. Geophysical Journal International 166, 1347–1362.
Biggs, J., Robinson, D.P., Dixon, T.H., 2009. The 2007 Pisco, Peru, earthquake (M8.0): seismology and geodesy. Geophysical Journal International 176, 657–669.
Biggs, J., Nissen, E., Craig, T., Jackson, J., Robinson, D.P., 2010. Breaking up the hanging wall of a rift-border fault: the 2009 Karonga earthquakes, Malawi. Geophysical Research Letters 37, L11305.
Burgmann, R., Rosen, P.A., Fielding, E.J., 2000. Synthetic aperture radar interferometry to measure Earth's surface topography and its deformation. Annual Reviews Earth and Planetary Sciences 28, 169–209.
Bustin, A., Hyndman, R., Lambert, A., Ristau, J., He, J., Dragert, H., Van der Kooij, M., 2004. Fault parameters of the Nisqually earthquake determined from moment tensor solutions and the surface deformation from GPS and InSAR. Bulletin of the Seismological Society of America 94, 363–376.
Cakir, Z., Chabalier, J.B.d., Armijo, R., Meyer, B., Barka, A., Peltzer, G., 2003. Coseismic and early post-seismic slip associated with the 1999 Izmit earthquake (Turkey), from SAR interferometry and tectonic field observations. Geophysical Journal International 155, 93–110.
Cattin, R., Briole, P., Lyon-Caen, H., Bernard, P., Pinettes, P., 1999. Effects of superficial layers on coseismic displacements for a dip-slip fault and geophysical implications. Geophysical Journal International 137, 149–158.
Chlieh, M., Chabalier, J.B.d., Ruegg, J.C., Armijo, R.D., Dmowska, R., Campos, J., Feigl, K.L., 2004. Crustal deformation and fault slip during the seismic cycle in the North Chile subduction zone, from GPS and InSAR observations. Geophysical Journal International 158, 685–711.
Cohee, B.P., Beroza, G.C., 1994. Slip distribution of the 1992 Landers earthquake and its implications for earthquake source mechanics. Bulletin of the Seismological Society of America 84, 692–712.
Cotton, F., Campillo, M., 1995. Frequency domain inversion of strong motions: application to the 1992 Landers earthquake. Journal of Geophysical Research 100, 3961–3975.
Curlander, J.C., McDonough, R., 1991. Synthetic Aperture Radar Systems and the Signal Processing. John Wiley and Sons.
Das, S., Scholz, C., 1983. Why large earthquakes do not nucleate at shallow depths. Nature 305, 621–623.
Dawson, J., Tregoning, P., 2007. Uncertainty analysis of earthquake source parameters determined from InSAR: a simulation study. Journal of Geophysical Research 112, B09406.
Decriem, J., Arnadottir, T., Hooper, A., Geirsson, H., Sigmundsson, F., Keiding, M., Ofeigsson, B.G., Hreinsdottir, S., Einarsson, P., LaFemina, P., Bennett, R.A., 2010. The 2008 May 29 earthquake doublet in SW Iceland. Geophysical Journal International 181, 1128–1146.
Delouis, B., Giardini, D., Lundgren, P., Salichon, J., 2002. Joint inversion of InSAR, GPS, teleseismic, and strong-motion data for the spatial and temporal distribution of earthquake slip: application to the 1999 Izmit mainshock. Bulletin of the Seismological Society of America 92, 278–299.
Delouis, B., Nocquet, J.M., Vallee, M., 2010. Slip distribution of the February 27, 2010 Mw = 8.8 Maule earthquake, central Chile, from static and high-rate GPS, InSAR and broadband teleseismic data. Geophysical Research Letters 37, L17305.
Doin, M.P., Lasserre, C., Peltzer, G., Cavalie, O., Doubre, C., 2009. Corrections of stratified tropospheric delays in SAR interferometry: validation with global atmospheric models. Journal of Applied Geophysics 69, 35–50.

Dziewonski, A.M., Woodhouse, J.H., 1983. An experiment in systematic study of global seismicity: centroid-moment tensor solutions for 201 moderate and large earthquakes of 1981. Journal of Geophysical Research 88, 3247–3271.
Dziewonski, A.M., Woodward, R., 1992. Acoustic imaging on the planetary scale. Acoustical Imaging 19, 785–797.
Dziewonski, A.M., Chou, T.A., Woodhouse, J.H., 1981. Determination of earthquake source parameters from waveform data for studies of global and regional seismicity. Journal of Geophysical Research 86, 2825–2852.
Eberhart-Philips, D., Stuart, W., 1992. Material heterogeneity simplifies the picture: Loma Prieta. Bulletin of the Seismological Society of America 82, 1964–1968.
Engdahl, E., van der Hilst, R., Buland, R., 1998. Global teleseismic earthquake relocation with improved travel times and procedures for depth determination. Bulletin of the Seismological Society of America 88, 722–743.
ESA, 2007. Sentinel-1 the radar mission for GMES operational land and sea services. ESA Bulletin 131.
ESA, 2011. ESA's Sentinel Satellites. http://www.esa.int/esaLP/SEMBRS4KXMF_LPgmes_0.html, 2011, Last Accessed, 26/04/11.
Feigl, K.L., 2002. Estimating earthquake source parameters from geodetic measurements. International Handbook of Earthquake and Engineering Seismology 81A, 1–14.
Feng, G., Hetland, E., Ding, X.L., Li, Z., Zhang, L., 2010. Coseismic fault slip of the 2008 Mw 7.9 Wenchuan earthquake estimated from InSAR and GPS measurements. Geophysical Research Letters 37, L01302.
Ferreira, A., Woodhouse, J.H., 2006. Long-period seismic source inversions using global tomographic models. Geophysical Journal International 166, 1178–1192.
Ferreira, A., Weston, J., Funning, G.J., 2011. Global compilation of interferometric synthetic aperture radar earthquake source models: 2. Effects of 3D earth structure. Journal of Geophysical Research 116, B08409.
Fialko, Y., 2004. Probing the mechanical properties of seismically active crust with space geodesy: study of the coseismic deformation due to the 1992 Mw 7.3 Landers (southern California) earthquake. Journal of Geophysical Research 109, B03307.
Fukushima, Y., Ozawa, T., Hashimoto, M., 2008. Fault model of the 2007 Noto Hanto earthquake estimated from PALSAR radar interferometry and GPS data. Earth Planets and Space 60, 99–104.
Funning, G.J., 2005. Source parameters of large shallow earthquakes in the Alpine–Himalayan belt from InSAR and waveform modelling. Ph.D. thesis. Faculty of Physical Sciences, University of Oxford.
Funning, G.J., Parsons, B., Wright, T.J., Jackson, J.A., Fielding, E.J., 2005. Surface displacements and source parameters of the 2003 Bam (Iran) earthquake from Envisat advanced synthetic aperture radar imagery. Journal of Geophysical Research 110, B09406.
Funning, G.J., Parsons, B., Wright, T.J., 2007. Fault slip in the 1997 Manyi, Tibet earthquake from linear elastic modelling of InSAR displacements. Geophysical Journal International 169, 988–1008.
Ghasemi, H., Fukushima, Y., Koketsu, K., Miyake, H., Wang, Z., Anderson, J.G., 2010. Ground-motion solution simulation for the 2008 Wenchuan. China, earthquake using the stochastic finite-fault method. Bulletin of the Seismological Society of America 100, 2476–2490.
Gilbert, F., Dziewonski, A.M., 1975. An Application of Normal Mode Theory to the Retrieval of Structural Parameters and Source Mechanisms from Seismic Spectra. Philosophical Transactions of the Royal Society of London.
Godey, A., Bossu, R., Guilbert, J., Mazet-Roux, G., 2006. The Euro-Mediterranean Bulletin: a comprehensive seismological bulletin at regional scale. Seismological Research Letters 77, 460–474.
Hao, K.X., Si, H., Fujiwara, H., Ozawa, T., 2009. Coseismic surface-ruptures and crustal deformations of the 2008 Wenchuan earthquake Mw 7.9, China. Geophysical Research Letters 36, L11303.
Hearn, E.H., Burgmann, R., 2005. The effect of elastic layering on inversions of GPS data for coseismic slip and resulting stress changes: strike-slip earthquakes. Bulletin of the Seismological Society of America 95, 1637–1653.
Hergert, T., Heidbach, O., 2006. New insights into the mechanism of postseismic stress relaxation exemplified by the 23 June 2001, Mw = 8.4 earthquake in southern Peru. Geophysical Research Letters 33.
Hutton, K., Woessner, J., Hauksoon, E., 2010. Earthquake monitoring in Southern California for seventy-seven years (1932–2008). Bulletin of the Seismological Society of America 100, 423–446.
IMD, 2011. Seismological Activities. http://www.imd.gov.in/section/seismo/static/welcome.htm2011Last accessed 23/05/11.
Jeffreys, H., Bullen, K., 1940. Seismological tables. British Association for the Advancement of Science 50.
Ji, C., Hayes, G., 2008. Preliminary Result of the May 12, 2008 mw 7.9 Eastern Sichuan, China Earthquake. (Last accessed 19/10/08).
Jonsson, S., Zebker, H., Segall, P., Amelung, F., 2002. Fault slip distribution of the 1999 Mw 7.1 Hector Mine, California, earthquake, estimated from satellite radar and GPS measurements. Bulletin of the Seismological Society of America 92, 1377–1389.
Jouanne, F., Awan, A., Madji, A., Pecher, A., Latif, M., Kausar, A., Mugnier, J.L., Khan, I., Khan, N.A., 2011. Postseismic deformation in Pakistan after the 8 October 2005 earthquake: evidence of afterslip along a flat north of the Balakot–Bagh thrust. Journal of Geophysical Research 116, B07401.
Kennett, B.L.N., Engdahl, E.R., Buland, R., 1995. Constraints on seismic velocities in the Earth from traveltimes. Geophysical Journal International 122, 108–124.
King, G.C.P., Stein, R., Lin, J., 1994. Static stress changes and the triggering of earthquakes. Bulletin of the Seismological Society of America 84, 935–953.
Kontoes, C., Elias, P., Sykioti, O., Briole, P., Remy, D., Sachpazi, M., Veis, G., Kotsis, I., 2000. Displacement field and fault model for the September 7, 1999 Athens earthquake inferred from ERS2 satellite radar interferometry. Geophysical Research Letters 27, 3989–3992.
Kubo, A., Fukuyama, E., Kawai, H., Nonomura, K., 2002. NIED seismic moment tensor catalogue for regional earthquakes around Japan: quality test and application. Tectonophysics 356, 23–48.
Li, Z., Muller, J.P., Cross, P., Fielding, E.J., 2005. Interferometric synthetic aperture radar (InSAR) atmospheric correction: GPS, Moderate Resolution Imaging Spectroradiometer (MODIS) and InSAR integration. Journal of Geophysical Research 110, B03410.
Li, X.J., Liu, L., Wang, Y.S., Yu, T., 2010. Analysis of horizontal strong-motion attenuation in the great 2008 Wenchuan earthquake. Bulletin of the Seismological Society of America 100, 2440–2449.
Liu-Zeng, J., Zhang, Z., Wen, L., Tapponnier, P., Sun, J., Xing, X., Hu, G., Xu, Q., Zeng, L., Ding, L., Ji, C., Hudnut, K.W., van der Woerd, J., 2009. Co-seismic rupture of the 12 May 2008, Ms 8.0 Wenchuan earthquake, Sichuan: east–west crustal shortening on oblique, parallel thrusts along the eastern edge of Tibet. Earth and Planetary Science Letters 286, 355–370.
Liu-Zeng, J., Wen, L., Sun, J., Zhang, Z., Hu, G., Xing, X., Zeng, L., Xu, Q., 2010. Surface slip and rupture geometry on the Beichuan Fault near Hongkou during the Mw 7.9 Wenchuan Earthquake, China. Bulletin of the Seismological Society of America 100, 2615–2650.
Lohman, R.B., Simons, M., 2005a. Locations of selected small earthquakes in the Zagros mountains. Geochemistry, Geophysics, Geosystems 6, Q03001.
Lohman, R.B., Simons, M., 2005b. Some thoughts on the use of InSAR data to constrain models of surface deformation: noise structure and data downsampling. Geochemistry, Geophysics, Geosystems 6, Q01007.
Lohman, R.B., Simons, M., Savage, B., 2002. Location and mechanism of the Little Skull Mountain earthquake as constrained by satellite radar interferometry and seismic waveform modelling. Journal of Geophysical Research 107, B6.
Marshall, G., Stein, R., Tatcher, W., 1991. Faulting geometry and slip from co-seismic elevation changes: the 18 October 1989, Loma Prieta, California, earthquake. Bulletin of the Seismological Society of America 81, 1660–1693.
Massonnet, D., Feigl, K.L., 1995. Satellite radar interferometric map of the coseismic deformation field of the M = 6.1 Eureka Valley, California earthquake of May 17, 1993. Geophysical Research Letters 22, 1541–1544.
Massonnet, D., Feigl, K.L., 1998. Radar interferometry and its application to changes in the earth's surface. Reviews of Geophysics 36, 441–500.
Massonnet, D., Rossi, M., Carmona, C., Adragna, F., Peltzer, G., Feigl, K., Rabaute, T., 1993. The displacement field of the Landers earthquake mapped by radar interferometry. Nature 364, 138–142.
McCaffrey, R., Abers, G., Zwick, P., 1991. Inversion of teleseismic bodywaves. In: Lee, W.H.K. (Ed.), IASPEI Software Library, 3, pp. 81–166.
Mellors, R.J., Magistrale, H., Earle, P., Cogbill, A., 2004. Comparison of four moderate-size earthquakes in Southern California using seismology and InSAR. Bulletin of the Seismological Society of America 94, 2004–2014.
Motagh, M., Wang, R., Walter, T., Burgmann, R., Fielding, E., Anderssohn, J., Zschau, J., 2008. Coseismic slip model of the 2007 August Pisco earthquake (Peru) as constrained by Wide Swath radar observations. Geophysical Journal International 174, 842–848.
Motagh, M., Schurr, B., Anderssohn, J., Cailleau, B., Walter, T., Wang, R., Vilotte, J.P., 2010. Subduction earthquake deformation associated with 14 November 2007, Mw 7.8 Tocopilla earthquake in Chile: results from InSAR and aftershocks. Tectonophysics 490, 60–68.
Nakamura, T., Tsuboi, S., Kaneda, Y., Yamanaka, Y., 2010. Rupture process of the 2008 Wenchuan, China earthquake inferred from teleseismic waveform inversion and forward modelling of broadband seismic waves. Tectonophysics 491, 72–84.
Nissen, E., Ghorashi, M., Jackson, J., Parsons, B., Talebian, M., 2007. The 2005 Qeshm Island earthquake (Iran) — a link between buried reverse faulting and surface folding in the Zagros Simply Folded Belt. Geophysical Journal International 171, 326–338.
Nissen, E., Yamini-Fard, F., Tatar, M., Gholamzadeh, A., Bergman, E., Elliot, J.R., Jackson, J.A., Parsons, B., 2010. The vertical separation of mainshock rupture and microseismicity at Qeshm Island in the Zagros fold-and-thrust belt, Iran. Earth and Planetary Science Letters 296, 181–194.
Okada, Y., 1985. Surface deformation due to shear and tensile fault in a half-space. Bulletin of the Seismological Society of America 75, 1135–1154.
Okada, Y., Kasahara, K., Hori, S., Obara, K., Sekiguchi, S., Fujiwara, H., Yamamoto, A., 2004. Recent progress of seismic observation networks in Japan — Hi-net, F-net, K-NET and KiK-net. Earth Planets and Space 56.
Ozawa, S., Yarai, H., Tobita, M., Une, H., Nishimura, T., 2008. Crustal deformation associated with the Noto Hanto Earthquake in 2007 in Japan. Earth Planets and Space 60, 95–98.
Peltzer, G., Rosen, P., 1995. Surface displacement of the 17 May 1993 Eureka Valley, California, earthquake observed by SAR interferometry. Science 268, 1333–1336.
Perfettini, H., Avouac, J.P., Tavera, H., Kositsky, A., Nocquet, J.M., Bondoux, F., Chlieh, M., Sladen, A., Audin, L., Farber, D.L., Soler, P., 2010. Seismic and aseismic slip on the Central Peru megathrust. Nature 465, 78–81.
Pondrelli, S., Morelli, A., Ekstrom, G., Mazza, S., Boschi, E., Dziewonski, A.M., 2002. European–Mediterranean regional centroid-moment tensors: 1997–2000. Physics of the Earth and Planetary Interiors 130, 71–101.
Pondrelli, S., Salimbeni, S., Morelli, A., Ekstrom, G., Olivieri, M., Boschi, E., 2010. Seismic moment tensors of the April 2009, L'Aquila (Central Italy) earthquake sequence. Geophysical Journal International 180, 238–242.
Pondrelli, S., Salimbeni, S., Morelli, A., Ekstrom, G., Postpischl, L., Vannuccii, G., Boschi, E., 2011. European–Mediterranean regional centroid moment tensor catalog: solutions for 2005–2008. Physics of the Earth and Planetary Interiors 185, 74–81.
Potin, P., 2011. Sentinal-1 Mission Overview. (Last Accessed 26/04/11).

Pritchard, M.E., Ji, C., Simons, M., 2006. Distribution of slip from 11 Mw > 6 earthquake in the northern Chile subduction zone. Journal of Geophysical Research 111, B10302.
Pussegur, B., Michel, R., Avouac, J.P., 2007. Tropospheric phase delay in interferometric synthetic aperture radar estimated from meteorological model multispectral imagery. Journal of Geophysical Research 112, B05419.
Rigo, A., de Chabalier, J.B., Meyer, B., Armijo, R., 2004. The 1995 Kozani–Grevena (northern Greece) earthquake revisited: an improved faulting model from synthetic radar interferometry. Geophysical Journal International 157, 727–736.
Rosen, P.A., Hensley, S., Joughin, I.R., Li, F.K., Madsen, S.N., Rodriguez, E., Goldtsein, R.M., 2000. Synthetic aperture radar interferometry. Proceedings of the IEEE 88.
Rosen, P.A., Hensley, S., Peltzer, G., 2004. Updated repeat orbit interferometry package released. EOS 85, 47.
Salichon, J., Lundgren, P., Delouis, B., Giardini, D., 2004. Slip history of the 16 October 1999 Mw 7.1 Hector Mine Earthquake (California) from the inversion of InSAR, GPS, and teleseismic data. Bulletin of the Seismological Society of America 94, 2015–2027.
Satyabala, S.P., 2006. Coseismic ground deformation due to an intraplate earthquake using synthetic aperture radar interferometry: the Mw 6.1 Killari, India, earthquake of 29 September 1993. Journal of Geophysical Research 111, B02302.
Satyabala, S.P., Bilham, R., 2006. Surface deformation and subsurface slip of the 28 March 1999 Mw = 6.4 west Himalayan Chamoli earthquake from InSAR analysis. Geophysical Research Letters 33, L23305.
Savage, J., 1987. Effect of crustal layering upon dislocation modeling. Journal of Geophysical Research 92, 10595–10600.
Savage, J., 1998. Displacement field for an edge dislocation in a layered half-space. Journal of Geophysical Research 103, 2439–2446.
Schmidt, D.A., Burgmann, R., 2006. InSAR constraints on the source parameters of the 2001 Bhuj earthquake. Geophysical Research Letters 33, L02315.
Sieh, K., Jones, L., Hauksoon, E., Hudnut, K., Eberhart-Philips, D., Heaton, T., Hough, S., Hutton, K., Kanamori, H., Lilje, A., Lindvall, S., McGill, S.F., Mori, J., Rubin, C., Spotila, J.A., Stock, J., Thio, H.K., Treiman, J.A., Wernicke, B., Zachariasen, J., 1993. Near-field investigations of the Landers earthquake sequence, April to July 1992. Science 260, 171–176.
Simons, M., Fialko, Y., Rivera, L., 2002. Coseismic deformation from the 1999 Mw 7.1 Hector Mine, California, Earthquake as inferred from INSAR and GPS observations. Bulletin of the Seismological Society of America 92, 1390–1402.
Smith, G.P., Ekstrom, G., 1996. Improving teleseismic event locations using a three-dimensional Earth model. Bulletin of the Seismological Society of America 86, 788–796.
Smith, G.P., Ekstrom, G., 1997. Interpretation of earthquake epicenter and CMT centroid locations, in terms of rupture length and direction. Physics of the Earth and Planetary Interiors 102, 123–132.
Sudhaus, H., Jonsson, S., 2009. Improved source modelling through combined use of InSAR and GPS under consideration of correlated data errors: application to the June 2000 Kleifarvatn earthquake Iceland. Geophysical Journal International 176, 389–404.
Sun, J., Shen, Z., Xu, X., Burgmann, R., 2008. Synthetic normal faulting of the 9 January 2008 Nima (Tibet) earthquake from conventional and along-track SAR interferometry. Geophysical Research Letters 35, L22308.
Swenson, J.L., Beck, S.L., 1999. Source characteristics of the 12 November 1996 Mw 7.7 Peru subduction zone earthquake. Pure and Applied Geophysics 154, 731–751.
Syracuse, E.M., Abers, G.A., 2009. Systematic biases in subduction zone hypocenters. Geophysical Research Letters 36, L10303.
Tahayt, A., Feigl, K.L., Mourabit, T., Rigo, A., Reilinger, R., McClusky, S., Fadil, A., Berthier, E., Dorbath, L., Serroukh, M., Gomez, F., Ben Sari, D., 2009. The Al Hoceima (Morocco) earthquake of 24 February 2004, analysis and interpretation of data from ENVISAT ASAR and SPOT5 validated by ground-based observations. Remote Sensing of the Environment 113, 306–316.
Talebian, M., Biggs, J., Bolourchi, M., Copley, A., Ghassemi, A., Ghorashi, M., Hollingsworth, J., Jackson, J., Nissen, E., Oveisi, B., Priestly, K., Saiidi, A., 2006. The Dahuiyeh (Zarand) earthquake of 2005 February 22 in central Iran: reactivation of an intramountain reverse fault. Geophysical Journal International 164, 137–148.
Treiman, J.A., Kendrick, K.J., Bryant, A., Rockwell, T.K., McGill, S.F., 2002. Primary surface rupture associated with the Mw 7.1 16 October 1999 Hector Mine Earthquake, San Bernardino County, California. Bulletin of the Seismological Society of America 92, 1171–1191.
United States Geological Survey (California Geological Survey), 2006. Quaternary Fault and Fold Database for the United States. http://earthquake.usgs.gov/hazards/qfaults, 2006, Last Accessed, 25/02/11.
Vannuccii, G., Gasperini, P., 2003. A database of revised fault plane solutions for Italy and surrounding regions. Computer & Geosciences 29, 903–909.
Velasco, A.A., Ammon, C.J., Farrell, J., Pankow, K., 2004. Rupture directivity of the 3 November 2002 Denali Fault Earthquake determined from surface waves. Bulletin of the Seismological Society of America 94, S293–S299.
Wadge, G., Zhu, M., Holley, R.J., James, I.N., Clark, P.A., Wang, C., Woodage, M.J., 2010. Correction of atmospheric delay effects in radar interferometry using a nested mesoscale atmospheric model. Journal of Applied Geophysics 84, 537–546.
Wald, D., Graves, R., 2001. Resolution analysis of finite fault source inversion using one- and three-dimensional Green's functions 2. Combining seismic and geodetic data. Journal of Geophysical Research 106, 8767–8788.
Wald, D., Heaton, T., 1994. Spatial and temporal distribution of slip for the 1992 Landers, California earthquake. Bulletin of the Seismological Society of America 84, 668–691.
Walters, R.J., Elliot, J.R., D'Agostino, N., England, P.C., Hunstad, I., Jackson, J.A., Parsons, B., Phillips, R.J., Roberts, G., 2009. The 2009 L'Aquila earthquake (central Italy): a source mechanism and implications for seismic hazard. Geophysical Research Letters 36, L17312.
Weston, J., Ferreira, A., Funning, G.J., 2011. Global compilation of InSAR earthquake source models: 1. Comparisons with seismic catalogs. Journal of Geophysical Research 116, B08408.
Wright, T.J., 2000. Crustal Deformation in Turkey from Synthetic Aperture Radar Interferometry. Ph.D. thesis. Faculty of Physical Sciences, University of Oxford.
Wright, T.J., Parsons, B.E., Jackson, J.A., Haynes, M., Fielding, E.J., England, P.C., Clarke, P.J., 1999. Source parameters of the 1 October 1995 Dinar (Turkey) earthquake from SAR interferometry and seismic bodywave modelling. Earth and Planetary Science Letters 172, 23–37.
Wright, T.J., Lu, Z., Wicks, C., 2003. Source model for the Mw 6.7, 23 October 2002, Nenana Mountain Earthquake (Alaska) from InSAR. Geophysical Research Letters 30, 1974.
Wright, T.J., Lu, Z., Wicks, C., 2004a. Constraining the slip distribution and fault geometry of the Mw 7.9, 3 November 2002, Denali Fault Earthquake with interferometric synthetic aperture radar and global positioning system data. Bulletin of the Seismological Society of America 94, 175–189.
Wright, T.J., Parsons, B.E., Lu, Z., 2004b. Toward mapping surface deformation in three dimensions using InSAR. Geophysical Research Letters 31.
Yagi, Y., Kikuchi, M., 2000. Source rupture process of the Kocaeli, Turkey, earthquake of August 17 1999, obtained by joint inversion of near-field data and telelseismic data. Geophysical Research Letters 27, 1969–1972.
Zhang, H., Ge, Z., 2010. Tracking the rupture of the 2008 Wenchuan earthquake by using the relative back-projection method. Bulletin of the Seismological Society of America 100, 2551–2560.